Plant Physiology®

Gene co-expression reveals the modularity and integration of C$_4$ and CAM in *Portulaca*

Ian S. Gilman [ID] ,[1,*] Jose J. Moreno-Villena [ID] ,[1] Zachary R. Lewis [ID] ,[1,‡] Eric W. Goolsby [ID] [2] and Erika J. Edwards [ID] [1,†]

1   Department of Ecology and Evolutionary Biology, Yale University, New Haven, Connecticut, USA
2   Department of Biology, University of Central Florida, Orlando, Florida, USA

*Author for correspondence: ian.gilman@yale.edu
†Senior author
‡Present address: Nanostring Technologies, Seattle, Washington, USA.
I.S.G. designed and conducted the experiments, analyzed the data, and wrote the article with contributions from all authors; J.J.M-.V. provided technical assistance with experiments and RNAseq data analysis; Z.R.L. assisted with data analysis and genome annotation methodology; E.W.G. and E.J.E. conceived of the original research plans, aided in experimental design, and supervised the writing. I.S.G. agrees to serve as the author responsible for contact and ensures communication.
The author responsible for distribution of materials integral to the findings presented in this article in accordance with the policy described in the Instructions for Authors (https://academic.oup.com/plphys/pages/general-instructions) is Ian S. Gilman (ian.gilman@yale.edu).

Abstract

C$_4$ photosynthesis and Crassulacean acid metabolism (CAM) have been considered as largely independent adaptations despite sharing key biochemical modules. *Portulaca* is a geographically widespread clade of over 100 annual and perennial angiosperm species that primarily use C$_4$ but facultatively exhibit CAM when drought stressed, a photosynthetic system known as C$_4$ + CAM. It has been hypothesized that C$_4$ + CAM is rare because of pleiotropic constraints, but these have not been deeply explored. We generated a chromosome-level genome assembly of *Portulaca amilis* and sampled mRNA from *P. amilis* and *Portulaca oleracea* during CAM induction. Gene co-expression network analyses identified C$_4$ and CAM gene modules shared and unique to both *Portulaca* species. A conserved CAM module linked phosphoenolpyruvate carboxylase to starch turnover during the day–night transition and was enriched in circadian clock regulatory motifs in the *P. amilis* genome. Preservation of this co-expression module regardless of water status suggests that *Portulaca* constitutively operate a weak CAM cycle that is transcriptionally and posttranscriptionally upregulated during drought. C$_4$ and CAM mostly used mutually exclusive genes for primary carbon fixation, and it is likely that nocturnal CAM malate stores are shuttled into diurnal C$_4$ decarboxylation pathways, but we found evidence that metabolite cycling may occur at low levels. C$_4$ likely evolved in *Portulaca* through co-option of redundant genes and integration of the diurnal portion of CAM. Thus, the ancestral CAM system did not strongly constrain C$_4$ evolution because photosynthetic gene networks are not co-regulated for both daytime and nighttime functions.

Introduction

Modularity and evolvability have become central research areas in biology over the past three decades (Wagner and Altenberg, 1996; Clune et al., 2013). Modularization

generates simple building blocks that facilitate rapid and complex adaptations through the combination of more discrete functions and the ability of simpler units to explore mutational space with minimal pleiotropic effects (Wagner and Altenberg, 1996; Lenski et al., 2003; Kashtan and

Alon, 2005; Kashtan et al., 2007; Clune et al., 2013). Modern "-omics" strategies have enabled detailed resolution of gene regulation in diverse study systems, and modeling results have shown that carbon metabolic networks have high potential for exaptation into evolutionary innovations in bacteria (Barve and Wagner, 2013). Empirical research has identified deeply conserved carbon metabolic modules from anaplerotic pathways that have been repeatedly recruited into plant photosynthetic adaptations known as carbon concentrating mechanisms (CCMs) (Heyduk et al., 2019). CCMs provide classic examples of rapid, adaptive evolution through the exaptation of existing metabolic modules that are subsequently refined for new functions.

Since the early Oligocene, CCMs—typically taking the form of C_4 photosynthesis or Crassulacean acid metabolism (CAM)—have evolved many dozens, if not hundreds, of times independently (Keeley and Rundel, 2003; Edwards et al., 2010; Christin et al., 2011; Sage, 2016; Edwards, 2019). Certain facets of CCMs, such as the main biochemical pathways, are evolutionarily accessible to all green plant lineages because they belong to deeply conserved photosynthetic and respiratory gene networks (Bräutigam et al., 2017; Heyduk et al., 2019). It is thought that by coupling these gene networks to light responses (C_4) (Hibberd and Covshoff, 2010) and circadian oscillators (CAM) (Hartwell, 2006), CCMs create two-stage carbon fixation pathways that address the most fundamental ecophysiological tradeoff in land plants: balancing CO_2 influx with water loss to transpiration.

Most plants assimilate carbon using C_3 photosynthesis, in which CO_2 is directly fixed by ribulose-1,5-bisphosphate carboxylase/oxygenase (RuBisCO) during the day in mesophyll cells. However, RuBisCO can also bind to O_2, triggering a set of costly reactions called photorespiration, which is exacerbated by hot, dry conditions (Peterhansel et al., 2010). CCMs increase the efficiency of photosynthesis by increasing the concentration of CO_2 around RuBisCO. This is achieved by first fixing carbon with phosphoenolpyruvate carboxylase (PEPC), which is either spatially (C_4) or temporally (CAM) decoupled from final fixation of CO_2 by RuBisCO (Figure 1, A and B). In both CCMs, CO_2 is first captured by beta carbonic anhydrase (BCA) and PEPC, forming oxaloacetate (OAA) (Figure 1, A and B) in the mesophyll, but exclusively during the night in CAM (Figure 1B). In CAM, OAA is then reduced to malate by malate dehydrogenase (MDH) and stored in the vacuole overnight as malic acid. During the day, CAM plants limit gas exchange with the external environment, and instead decarboxylate stored malate with malic enzymes (MEs) to release CO_2. Most C_4 species also reduce OAA to malate (NADP-type biochemistry), but others first transaminate it to produce aspartate (NAD-type biochemistry) via aspartate aminotransferase (ASP). These 4-carbon acids are transported to the bundle-sheath cells and decarboxylated. In NAD-type C_4 species, ASP reversibly transforms aspartate back into OAA in bundle-sheath mitochondria, where it is reduced to form malate by NAD-

dependent MDH (NAD-MDH) and finally decarboxylated by NAD-dependent ME (NAD-ME). By separating initial CO_2 capture in the mesophyll from assimilation in the bundle sheath, C_4 increases photosynthetic rates and water-use efficiency while minimizing energy and carbon lost to photorespiration (Ogren, 1984; Sage, 2004; Taylor et al., 2014). CAM does not always reduce photorespiration (Niewiadomska and Borland, 2008; Lüttge, 2011), but greatly increases water-use efficiency (Szarek and Ting, 1975; Winter et al., 2005) and reduces the harmful effects of high heat and radiation caused by oxidative stress (Niewiadomska and Borland, 2008).

C_4 and CAM boost the efficiency of photosynthesis in different ways and are, therefore, hypothesized to have evolved in response to different stressors. C_4 has been primarily considered as an adaptation to high rates of photorespiration (Ehleringer et al., 1997; Sage et al., 2012), and CAM to water limitation (Raven and Spicer, 1996; Keeley and Rundel, 2003), though photorespiratory and drought stress are often experienced simultaneously (Arakaki et al., 2011). Given the overlapping environmental contexts of CAM and C_4 evolution, their repeated assembly of a similar set of biochemical modules (Christin et al., 2014; Heyduk et al., 2019) (Figure 1, A and B), and their apparent ease of evolution, it is perhaps surprising that use of both C_4 and CAM (hereafter C_4 + CAM) has only been reported in four lineages: *Portulaca* (Portulacaceae) (Koch and Kennedy, 1980), *Ottelia* (Hydrocharitaceae) (Huang et al., 2018), *Spinifex* (Poaceae) (Ho et al., 2019), and *Trianthema* (Aizoaceae) (Winter et al., 2020). On the other hand, it may be precisely the large overlap in CCM gene networks and metabolites that may make C_4 and CAM mutually exclusive in most lineages (Sage, 2002). Plants that use both C_4 and CAM seemingly must regulate the same gene networks in contrasting patterns that may result in futile metabolite cycling and inefficient transport. For example, daytime decarboxylation activity in the mesophyll during CAM would directly oppose C_4 carboxylation activity.

Portulaca, a geographically widespread clade of over 100 annual and perennial herbs and small shrubs, predominantly use C_4, but facultatively exhibit CAM in response to drought (Koch and Kennedy, 1980, 1982; Guralnick and Jackson, 2001; Guralnick et al., 2002; Lara et al., 2003, 2004; Christin et al., 2014; Holtum et al., 2017; Winter et al., 2019; Ferrari et al., 2020b, 2020c). It has been hypothesized that their CAM cycle must be either spatially separated from the C_4 cycle, that is, relegated to a subpopulation of leaf cells such as water storage or bundle sheath (Guralnick et al., 2002; Sage, 2002); or alternatively, that *Portulaca* operate a novel two cell CAM system, whereby CAM malate is decarboxylated in the bundle sheath (Lara et al., 2003, 2004). Facultative CAM, the reversible induction of CAM in response to drought stress, is assumed to be ancestral in *Portulaca* because it has been observed in every major subclade assayed (Holtum et al., 2017; Winter et al., 2019) as well as in *Portulaca*'s closest relatives (Edwards and Diaz,
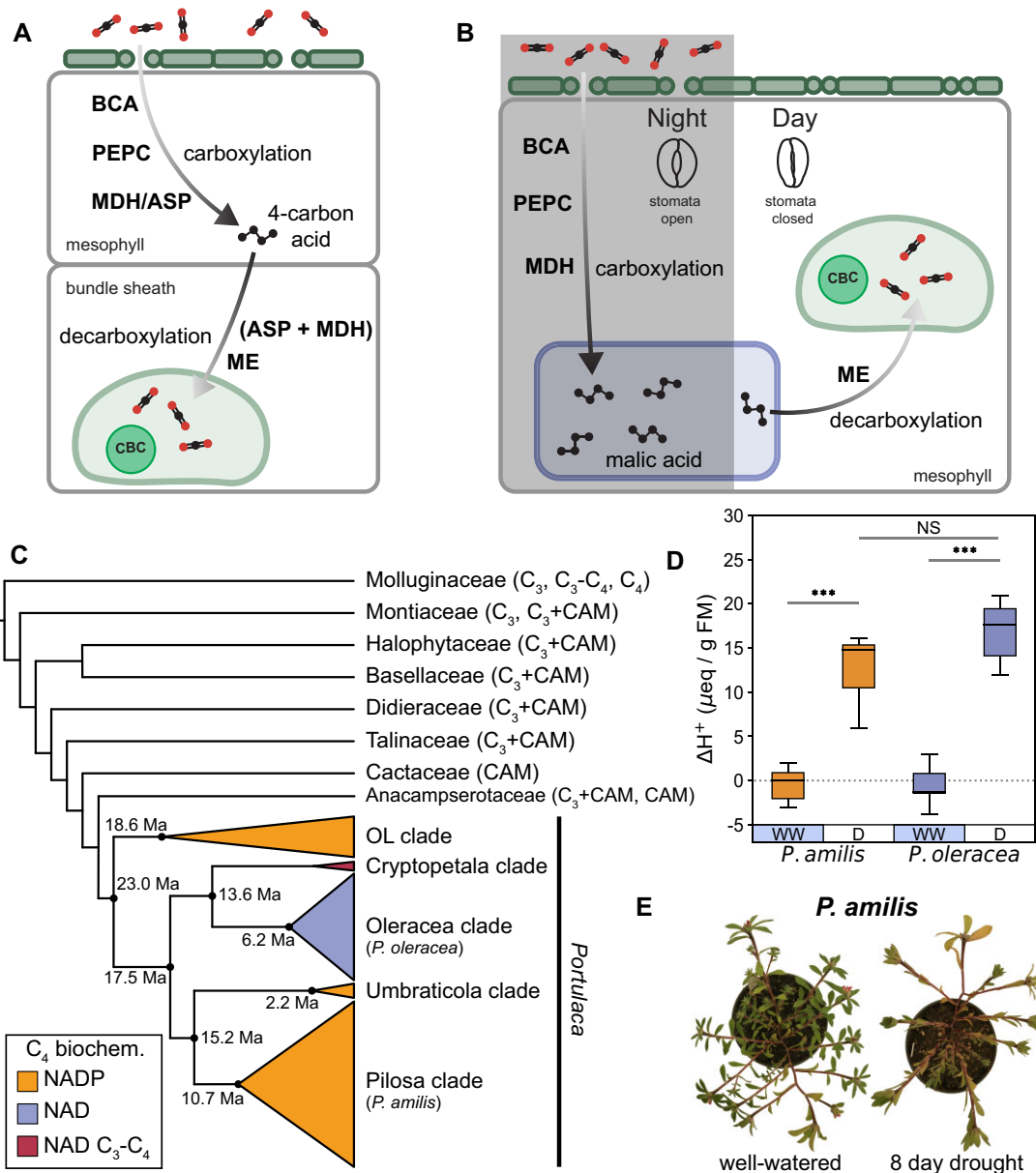
Figure 1 Overview of CCMs in the Portullugo. Simplified C$_4$ (A) and CAM (B) pathways showing shared carboxylation and decarboxylation pathways. ASP, aspartateaminotransferase; BCA, beta carbonic anhydrase; CBC, Calvin–Benson cycle; MDH, malate dehydrogenase; ME, malic enzyme; PEPC, PEP carboxylase. Cartoon dendrogram of the Portullugo (Portulacineae + Molluginaceae), highlighting major *Portulaca* clades (C), which are colored by primary C$_4$ biochemical pathway. Mean age estimates for focal *Portulaca* clades are from Ocampo and Columbus (2012). Boxplots of night-day differences in titratable acidity ($n = 6$) of experimental *P. amilis* (orange) and *P. oleracea* plants (purple) (D); boxplots show median and interquartile range; whiskers show 1.5 × interquartile range. WW, well-watered; D, drought. Asterisks connecting lines indicate significant differences between well-watered and drought treatments (independent t test; "***", $P < 0.001$; "NS", $P = 0.121$). Images of *P. amilis* when well-watered and after 8 days without water (E); images were digitally extracted for comparison.

2006; Guralnick et al., 2007; Brilhaus et al., 2016; Holtum et al., 2018; Hancock et al., 2019; Holtum et al., 2021) (Figure 1C). Transcriptomic studies of *Portulaca* and its close relatives suggest that the ancestral CAM pathway used both NAD- and NADP-type enzymes for CAM (Brilhaus et al., 2016; Ferrari et al., 2020b, 2020c). The biochemical diversity of C$_4$ pathways in major *Portulaca* clades and the observation of intermediate photosynthetic phenotypes (C$_3$–C$_4$) in

the Cryptopetala clade (Ocampo et al., 2013; Voznesenskaya et al., 2017; Winter et al., 2019) imply multiple origins of C$_4$ within a facultative CAM context (Figure 1C). Multiple C$_4$ origins are further evidenced by differences in leaf ultrastructure among lineages (Voznesenskaya et al., 2010, 2017; Ocampo et al., 2013), as Kranz anatomy is typically established early in C$_4$ evolution (Sage et al., 2012; Williams et al., 2013).

Photosynthetic gene activity has only been studied in detail in *Portulaca oleracea* (Ferrari et al., 2020b, 2020c), an NAD-type species. Similar experiments on other *Portulaca* are needed to answer fundamental questions about the function and evolution of C_4 + CAM, and the integration of metabolic modules more generally. Facultative CAM is hypothesized to be ancestral to *Portulaca*, but expression of CAM-specific orthologs in multiple species has not yet been documented. And although multiple carboxylation and decarboxylation pathways can co-exist in some C_4 plants (Furbank, 2011), it is not obvious why or how different C_4 biochemistries would evolve in lineages that shared an ancestral, mixed CAM biochemistry type, nor do we know the extent to which these CCMs have been integrated in various lineages.

Here, we present a chromosome-level genome assembly of *Portulaca amilis* (NADP-type C_4), to our knowledge, the first of any C_4 + CAM plant. We analyzed transcriptomic data during a CAM-induction experiment to understand the synergistic evolution of multiple metabolic modules. Concurrent transcriptomic data for *P. oleracea* allowed us to compare C_4 + CAM systems across a deep split in the *Portulaca* phylogeny and discriminate between ancestral, inherited, and lineage-specific gene networks. We confirm previous hypotheses that *Portulaca* species share one CAM-specific PEPC ortholog (*PPC-1E1c*) and another C_4-specific ortholog (*PPC-1E1a′*) (Christin et al., 2014), and provide evidence that CAM evolved by linking PEPC to starch catabolism and altering *PEPC kinase* expression in response to drought (Carter et al., 1996). We found some evidence for CAM-specific decarboxylation pathways, but the daytime part of CAM appears to have been largely integrated into C_4 metabolism, and we predict that nocturnal acids produced by CAM are likely shuttled into the diurnal pool of bundle-sheath C_4-acids. Finally, although *P. amilis* and *P. oleracea* share some central C_4 orthologs, exclusive use of orthologs from most core gene families highlights the diversity of C_4 + CAM systems and provides further evidence that C_4 evolved largely independently in multiple *Portulaca* lineages.

Results

CAM induction experiment

Significant diel fluctuations in titratable leaf acidity indicative of CAM activity and signs of drought stress—leaf yellowing, paraheliotropism (leaf orientation to minimize light absorption)—were observed after 7 and 8 days without water in *P. amilis* and *P. oleracea*, respectively (Figure 1, D and E). Diel fluctuations in titratable acidity were not significantly different from zero when well-watered (p_{amilis} = 0.624, $p_{oleracea}$ = 0.591), but were significantly different under drought (p_{amilis} = 0.00069, $p_{oleracea}$ = 0.00053), and significantly greater than when well-watered (Figure 1D). There was no significant difference between the magnitude of diel fluctuations between species (p = 0.121).

Genome and transcriptome assembly and annotation

The *P. amilis* v1 genome assembly was 403.89 Mb in length and extremely contiguous (L50/N50 = 5 scaffolds/42.598 Mb; L90/N90 = 9 scaffolds/39.183 Mb), with nine primary scaffolds representing the nine expected chromosomes of the haploid *P. amilis* genome (Figure 2A) based on the karyotype of a close relative (*Portulaca grandiflora*) (Sharma and Bhattacharyya, 1956). The scaffolds were 92.9% complete and single copy as measured by the BUSCO version 5 embryophyta database (C: 96.9% [S: 92.9%, D: 4.0%], F: 1.5%, M: 1.6%, n: 1,614). Slightly less than half of the assembly was masked as repetitive elements (46.96%), which primarily consisted of LTRs (41.96%), DNA elements (29.36%), and LINEs (13.85%) (Figure 2B). A repeat landscape of these elements did not show any sudden bursts of element activity or multiple peaks (Figure 2B), which can signify genomic upheaval from hybridization or polyploidy events (McClintock, 1984; Dion-Côté et al., 2014). The final annotation contained 53,094 gene models with 58,732 unique coding sequences (Figure 2C). This gene count is higher than expected given the size of the *P. amilis* genome, and may result from split gene models; however, it is also likely that more gene models are identified in more contiguous genomes, and when large and diverse transcriptomic evidence is used during the annotation process.

The *P. oleracea* de novo transcriptome assembly contained 413,658 transcripts corresponding to 230,086 "unigenes" (hereafter, "genes") that were highly complete but infrequently single copy: BUSCO version 5 embryophyta (C: 94.7% [S: 16.4%, D: 78.3%], F: 3.2%, M: 2.1%, n: 1,614). The high number of duplicate BUSCOs was expected, as most members of the *P. oleracea* species complex are polyploid (Ocampo and Columbus, 2012). Less than half of the transcripts (198,026) were predicted to be coding sequences, which corresponded to 45,285 genes.

A total of 21,621 *P. amilis* and 44,532 *P. oleracea* genes passed filtering for differential abundance analysis, and over half of these genes (*P. amilis*, 62%; *P. oleracea*, 51.0%) were found to be significantly differentially abundant between well-watered and drought conditions following Benjamini–Hochberg corrections (Benjamini and Hochberg, 1995) for false discovery (q < 0.01; see "Materials and methods").

Co-expression network analysis

The well-watered and drought *P. amilis* photosynthetic gene networks (PGNs) were similar in size and density but had different distributions of node degree due to a small number of extremely highly connected genes belonging to modules paWW1 and paWW3 (Figure 3A; Supplemental Figure S1C and Supplemental Table S1), which were characterized by C_4-like expression: very high morning abundance that rapidly tapered off by late afternoon. Indeed, paWW1 contained at least one homolog of all core elements of the C_4 pathway; including *PaPPC-1E1a′*, the C_4-specific *PPC* ortholog used by *P. oleracea* (Christin et al., 2014; Ferrari et al., 2020b, 2020c) (Figure 3C). The most similar drought module to paWW1 in
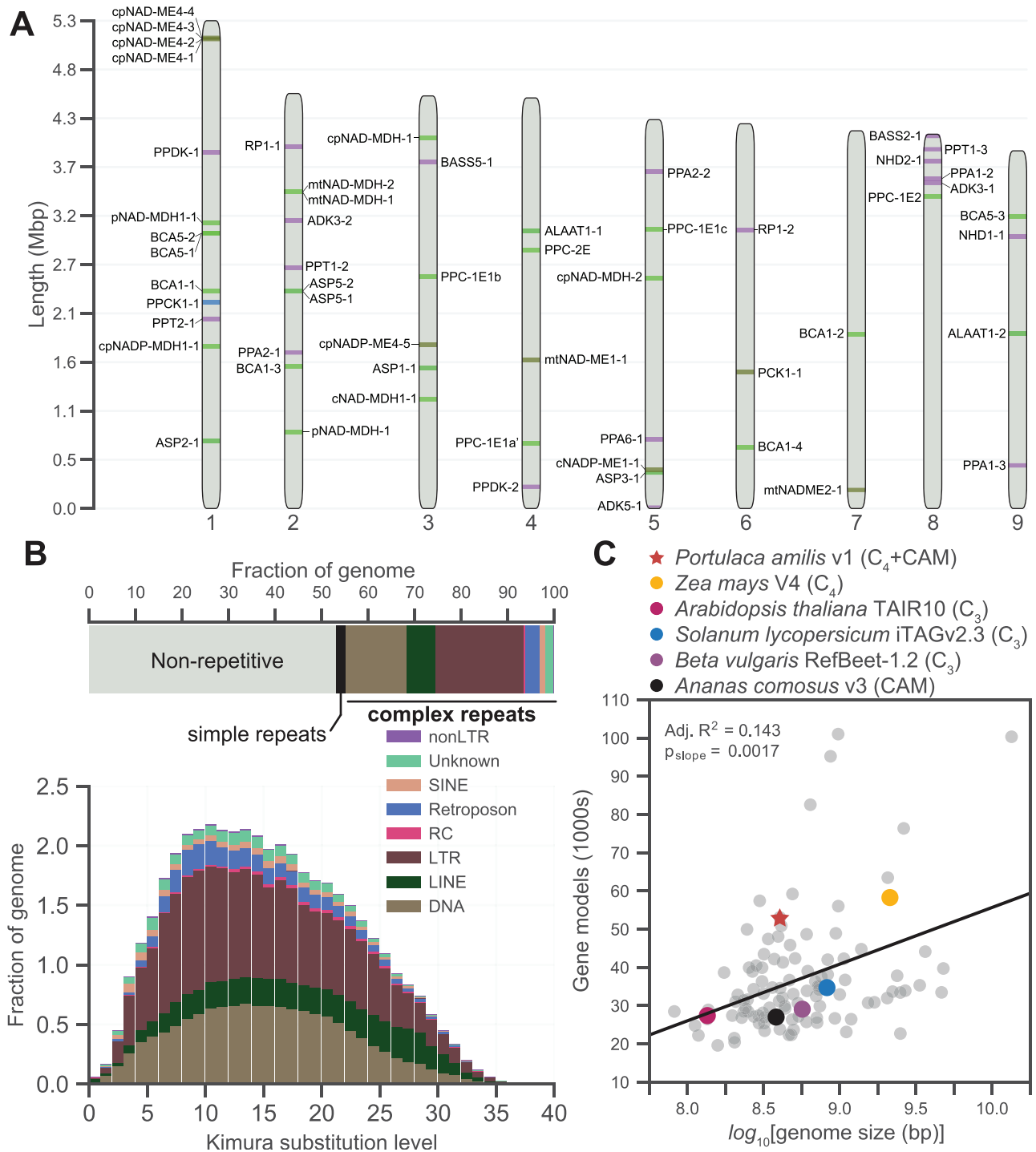
Figure 2 Genome and genomic content of *P. amilis*. Idiogram of the nine primary scaffolds of the *P. amilis* genome with key C₄ and CAM genes highlighted (A). Breakdown of repetitive elements (B); the horizontal bar chart shows the fractions of major classes of repetitive elements and the repeat landscape (histogram) shows the relative abundances of repetitive elements versus the Kimura substitution level from the consensus. Scatterplot of number of gene models versus the log10-transformed genome size for 107 angiosperm genomes (C) with notable benchmarking and CCM genomes highlighted; data are from Zhao and Schranz (2019). Line in (C) shows results of ordinary least squares regression; one sample t_{slope} (106) > 0, p_{slope} = 0.0017.

terms of constituent genes, paD6, was 31% smaller (72 genes), while the largest drought module (paD1) was characterized by dark period peak expression and consisted primarily of light response and circadian transcription factors

and starch catabolism-related genes (Figure 3B). The largest well-watered *P. oleracea* module (poWW2) also contained *PoPPC-1E1a'*; however, the *P. oleracea* transcriptome contained five *PoPPC-1E1a'* transcripts distributed between two
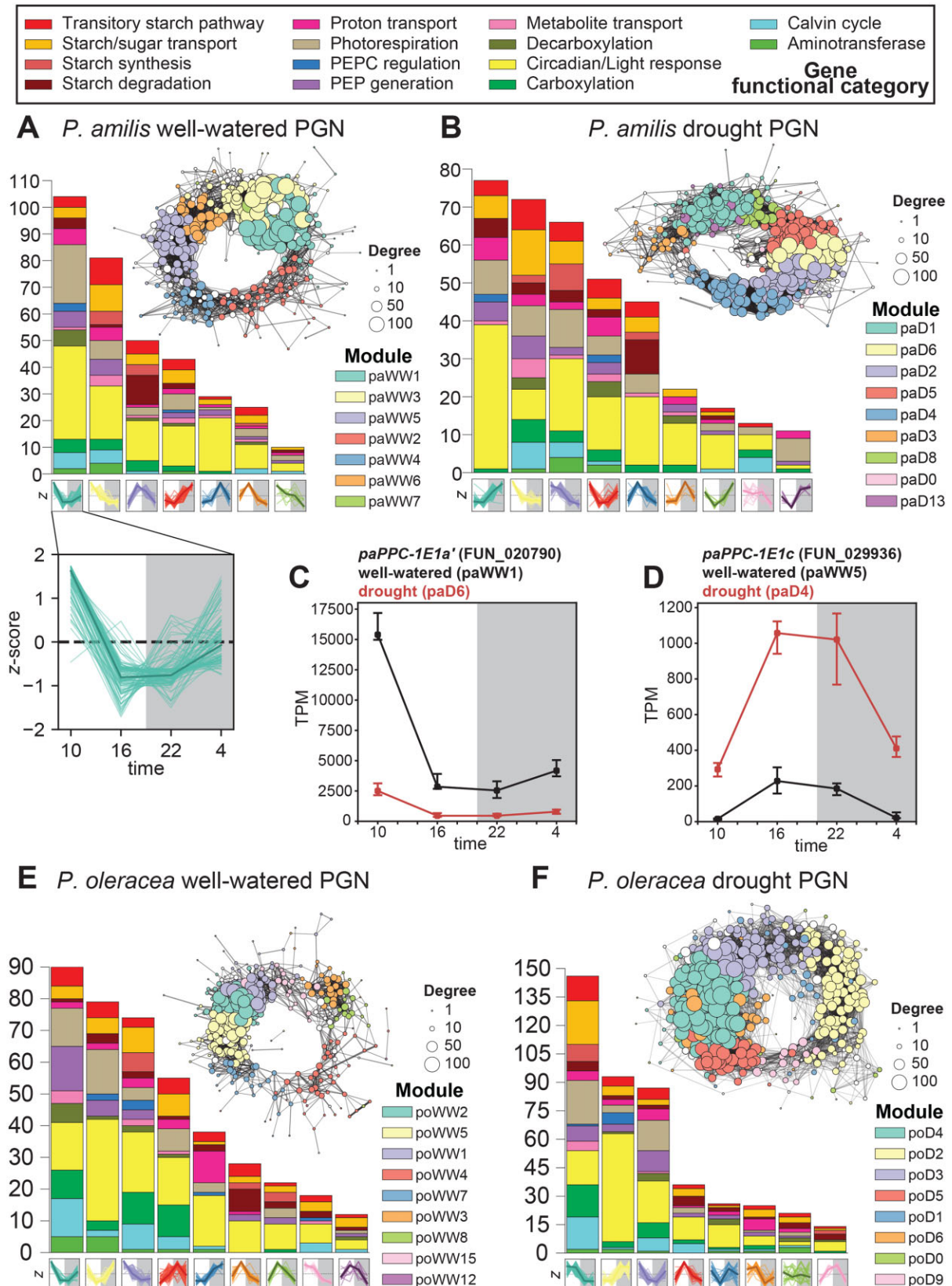
Figure 3 PGNs. Well-watered and drought PGNs of *P. amilis* (A and B), and *P. oleracea* (E and F) colored by WGCNA co-expression module identity. Each node in the graph represents one gene and node sizes represent their degrees. Each module's size and functional composition are shown in the histogram, and the *z*-score normalized expression of each module's constituent genes is shown along the horizontal axis. An example of the *z*-score normalized expression for module paWW1 is enlarged in (A) to show individual gene expression with the median highlighted in bold. TPM normalized expression profiles of two focal *PPC* transcripts (*PaPPC-1E1a'* and *PaPPC-1E1c*) are shown in (C) and (D), respectively; points show median of six biological replicates and error bars show interquartile range; black and red lines represent well-watered and drought samples, respectively.

modules with C_4-like expression (poWW2 and poWW1) (Figure 3E). There was a greater size discrepancy between the *P. oleracea* PGNs, and the drought PGN was much larger and denser than the well-watered PGN (Figure 3, E and F; Supplemental Table S1).

We expected the CAM cycle to be broken into two modules: one that builds PEP from transitory starches and carboxylates CO_2 into malate from dusk until dawn, and a second that decarboxylates malate into CO_2 for fixation by RuBisCO during the day (Figure 1B). As reported in *P. oleracea* (Christin et al., 2014; Ferrari et al., 2020b, 2020c), *P. amilis* used the *PPC* paralog *PaPPC-1E1c* for CAM (Figure 3D), and this gene belonged to smaller modules with abundance profiles that peaked across the light-dark transition, and which were dominated by starch degradation and circadian clock genes (paWW5 and paD4; Figure 3, A, B, and D). To identify genes that may be co-regulated for nocturnal use in CAM, we extracted genes that remained co-expressed (preserved) with *PaPPC-1E1c* across well-watered and drought conditions. Except for one photorespiratory gene (*catalase 1, PaCAT1-2*, FUN_025647), all had functions related to carboxylation (*PaPPC-1E1c* and *PaBCA1-2*), starch metabolism and catabolism (Figure 4, A–E), or circadian rhythm and light response. However, *PaBCA1-3* (FUN_009254) was more highly expressed than *PaBCA1-2* and upregulated under drought with peak nocturnal abundance (Figure 4H). At least one paralog of all members of the phosphorolytic starch degradation pathway were preserved, except alpha-amylase (*AMY*). The two most highly expressed *AMY* genes, *PaAMY3-2* (FUN_023174; paD1) and *PaAMY1-2* (FUN_018918; paD14), both increased in abundance under drought with nocturnal expression peaks. The most highly abundant (*PaAMY3-2*) exhibited CAM-like expression despite falling outside of module paD4 (Figure 4F), consistent with findings in CAM *Kalanchoë*, which uses AMY3 as the primary phosphorolytic starch degradation enzyme (Ceusters et al., 2021). One homolog of *BAM3* (*PaBAM3-2*, FUN_041354)—responsible for hydrolytic starch breakdown in C_3 species (Smith et al., 2005; Weise et al., 2011)—was recovered in the drought module but significantly downregulated (Figure 4G), as was *PaBAM3-1* (FUN_017370). One paralog of aluminum activated malate transporter 4 (*PaALMT4-2*, FUN_033599), which imports malate into the vacuole, was also recovered in drought module paD4 (Figure 4I). No *MDH* homologs were recovered in this nocturnal CAM network; however, *PaNAD-MDH-1* (FUN_01186) was significantly differentially abundant under drought with peak nocturnal abundance (Figure 4K), although it was not among the most highly abundant homologs. Most homologs were recovered in drought modules paD6, paD2, and paD5 with C_4-like expression (Supplementary Figure S2). Similarly, the expression of *MDH* in the facultative CAM plant *Isoetes taiwanensis* was not synchronous with *PPC* (Wickell et al., 2021). In total, 28 genes were preserved with *PaPPC-1E1c* (Figure 5A) and, except for *MDH*, at least one homolog of all CAM-related carboxylation and starch degradation genes

had correlated expression over the day–night transition or nocturnal expression peaks.

The *P. oleracea* transcriptome contained multiple transcripts of *PoPPC-1E1c* that were recovered in two well-watered modules (poWW4 and poWW8) and three drought modules (poD2, poD5, and poD9) that were consistent with use in CAM (Figure 3, E and F). The preserved genes were functionally similar to those preserved in the *P. amilis* nocturnal CAM network and were involved with starch metabolism and catabolism, and the circadian clock (Figure 5B). Among the genes preserved with *PoPPC-1E1c* was cytoplasmic *PoNAD-MDH1* (TRINITY_DN7462_c3_g1), which was the most highly expressed *NAD-MDH* under drought (Supplemental Fig. S3). Furthermore, many of the genes that link phosphorolytic starch degradation to PEP generation were preserved in the nocturnal CAM network, including *AMY*, *fructose-bisphosphate aldolase* (*FBA*), *glyceraldehyde-3-phosphate dehydrogenase* (*GAP*), and *phosphofructokinase* (*PFK*). Although not preserved, the *PoPPC-1E1c* drought modules included copies of phosphoglucomutase (*PGM*) and enolase (*ENO*), the final two steps in PEP generation from starch or soluble sugars.

We used the *PaPPC-1E1c* and *PoPPC-1E1c* drought modules to identify the set of genes common to both nocturnal CAM networks (Figure 5, C and D). By taking the intersection of the two sets of *PPC-1E1c* drought module genes (i.e. preserved and drought exclusive genes), we uncovered 21 *P. amilis* and 24 *P. oleracea* orthologs (some genes had multiple paralogs in the *P. oleracea* network). Congruent with facultative CAM metabolic models, which predict a transition from hydrolytic to phosphorolytic starch pathways coincident with CAM to save energy (Shameer et al., 2018), the orthologous nocturnal CAM networks contained one gene involved in starch synthesis (starch branching enzyme 3, *SBE3*), five phosphorolytic starch degradation genes, and alpha-glucan phosphorylase 2 (*PHS2*), which is also part of phosphorolytic starch metabolism and catabolism (Figure 5E). These networks therefore included much of the phosphorolytic starch degradation pathway that forms the basis of PEP generation in most CAM plants (Weise et al., 2011; Borland et al., 2016; Shameer et al., 2018; Ceusters et al., 2021), but many interactions differed between species (Figure 5, C and D). The largest group of shared genes were core circadian clock elements: *Adagio* (*ADO*), also known as *ZEITLUPE*, 1 and 3, two *Arabidopsis pseudo-response regulator 5* (*APRR5*) paralogs, *EARLY FLOWERING* (*ELF*) 1 and 4, *GIGANTEA* (*GI*), one *LUX ARRHYTHMO* (*LUX*) paralog, and one *REVEILLE 6* (*RVE6*) paralog (Figure 5, C–E). Although the two species' nocturnal CAM networks shared many key orthologs, there were notable differences. The *P. oleracea* network did not contain an *ALMT* homolog but did contain three paralogs of *PEPC kinase 1* (*PPCK1*) that were all highly abundant and significantly upregulated under drought ($q < 1.0 \times 10^{-7}$) (Supplemental Figure S3). PPCK increases the activity of PEPC, which is inhibited by malate, forming a negative feedback loop (Nimmo, 2000). While all three
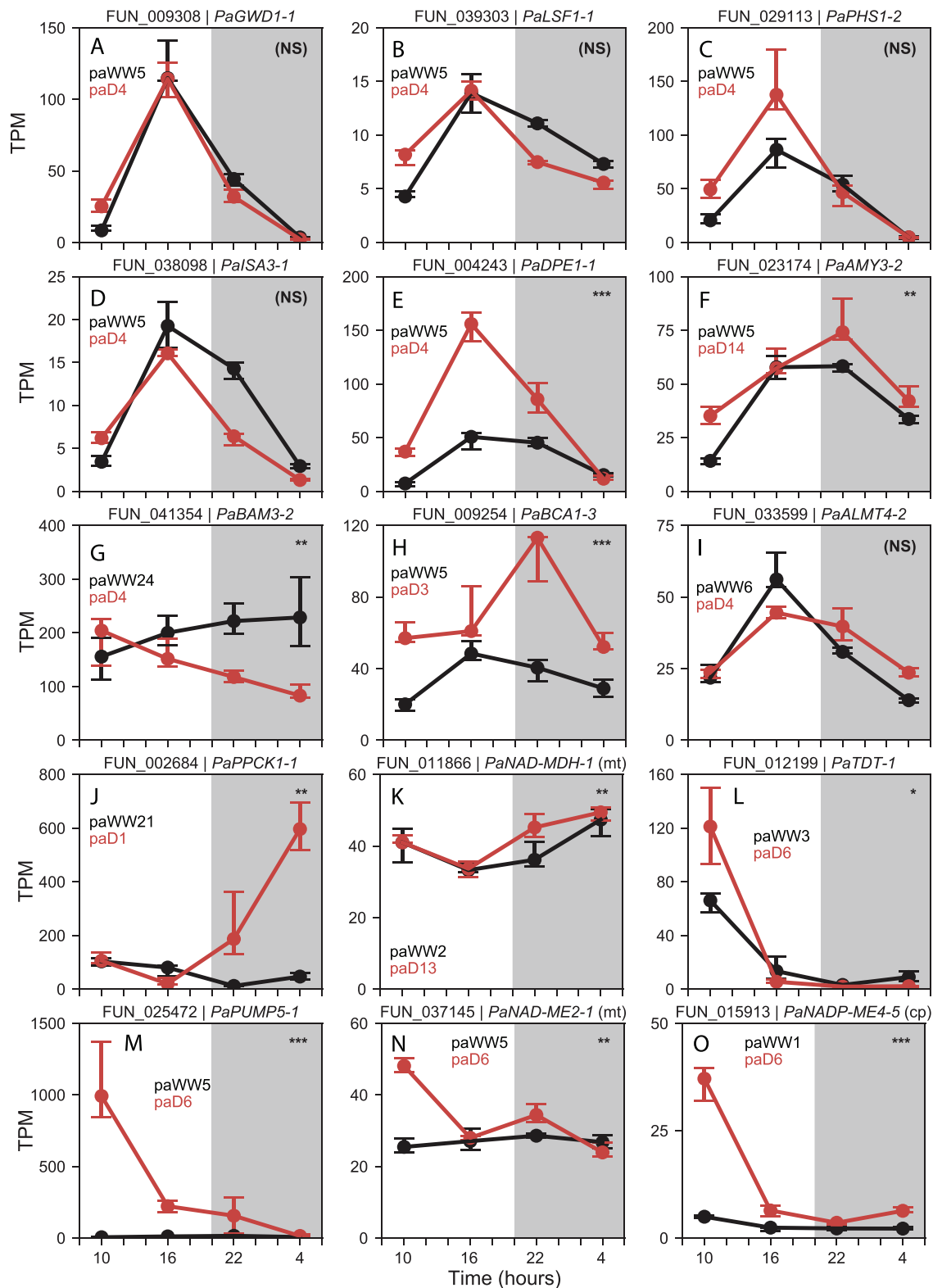
Figure 4 TPM normalized abundance of selected *P. amilis* genes hypothesized to be involved in CAM. Gene model and name are shown above each plot, and black and red lines show median well-watered and drought abundance of all biological replicates ($n = 6$), respectively; error bars show interquartile range. Module assignments are listed for well-watered and drought networks in black and red, respectively. (A) *GWD*, glucan water dikinase; (B) *LSF*, phosphoglucan phosphatase; (C) *PHS*; (D) *ISA*, isoamylase; (E) *DPE*, 4-alpha-glucanotransferase; (F) *AMY*; (G) *BAM*, beta-amylase; (H) *BCA*; (I) *ALMT*, aluminum-activated malate transporter; (J) *PPCK*, PEPC kinase; (K) *NAD-MDH*; (L) *TDT*; (M) *PUMP*, mitochondrial uncoupling protein/dicarboxylate carrier; (N) *NAD-ME*, NAD-dependent ME; (O) *NADP-ME*, NADP-dependent ME. Significant differences in abundance across each time series between well-watered and drought conditions are shown in the upper right corner of each plot. P-values for unique transcripts were aggregated for each gene model and transformed into q-values by adjusting for false discovery rate (see "Materials and methods"); "NS" = nonsignificant, "*" = $q < 0.05$, "**" = $q < 0.01$, "***" = $q < 0.001$.
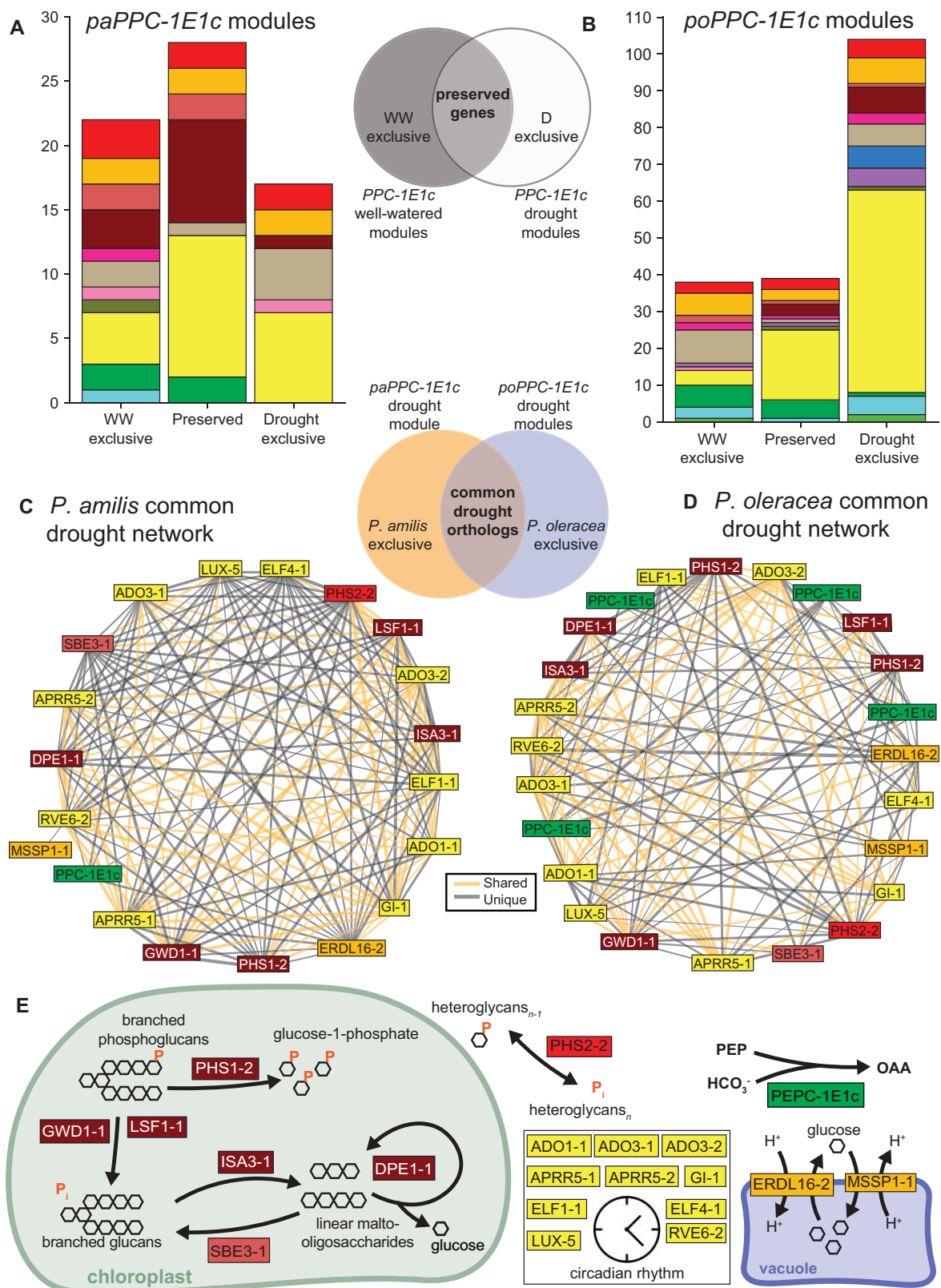
Figure 5 *PPC-1E1c* PGN preservation and subnetworks of common genes. Stacked bar charts showing the number and functional composition of genes that were exclusive to the well-watered or drought *PPC-1E1c* PGNs, or preserved across treatments in *P. amilis* (A) and *P. oleracea* (B). Subnetworks induced by genes common to both *P. amilis* (C) and *P. oleracea* (D) drought *PPC-1E1c* PGNs; drought PGNs include preserved and drought exclusive genes. Orange edges represent correlations among genes shared between species, while black edges are unique to each respective species. Metabolic pathways of the shared *PPC-1E1c* subnetworks (E), showing PEPC, sugar transport, and starch metabolism. PEP, phosphoenolpyruvate; OAA, oxaloacetate; ADO, Adagio; APRR, Arabidopsis pseudo-response regulator; DPE, 4-alpha-glucanotransferase; ELF, EARLY FLOWERING; GI GIGANTEA; GWD, glucan water dikinase; ISA, isoamylase; LSF, phosphoglucanphosphatase; LUX, LUX ARRHYTHMO; PHS, alpha-glucan phosphorylase; PEPC, PEP carboxylase; SBE, starch branching enzyme; RVE, REVEILLE. Colors of bar plot units (A and B) and gene boxes (C–E) indicate functional categories as in Figure 3.

PoPPCK transcripts were upregulated under drought with peak nighttime expression indicative of use in CAM, all had higher daytime levels of abundance under drought as well—which points toward a dual role in both C_4 and CAM. The single *PPCK* ortholog in *P. amilis* (FUN_002684) was also significantly more abundant under drought ($q = 0.0011$) with peak nocturnal expression (Figure 4J), but it was recovered in drought module paD1, which increased in abundance throughout the night (Figure 3B). This pattern, where *PPC* abundance peaks in the late afternoon followed by a sharp increase in *PPCK* late into the dark period mirrors the evolved expression patterns of other facultative and obligate CAM lineages, such as *Sedum* (Wai et al., 2019), *Isoetes* (Wickell et al., 2021), pineapple (*Ananas comosus*), and *Kalanchoë* (Yang et al., 2017). PPCK activity is typically essential for highly active CCMs, and a CAM-like expression pattern in *PaPPCK1* would suggest low PEPC activity during C_4. However, we found a derived amino acid residue, glutamic acid (E), in *PaPPC-1E1a′* at the same location where an aspartic acid (D) residue (D509) was demonstrated to reduce malate inhibition in *Kalanchoë* and *Phalaenopsis* orchids (Yang et al., 2017). In *Kalanchoë* and *Phalaenopsis*, the D509 residue was shown to be derived from either arginine (R), lysine (K), or histidine (H), the latter of which is present at position 509 in *PoPPC-1E1a′*. Glutamic acid is functionally similar to aspartic acid, and may similarly reduce malate inhibition; thus, allowing for high PEPC activity during C_4 without the need for PPCK.

We considered two modules each in *P. amilis* (paWW1 + paWW3 and paD5 + paD6) and *P. oleracea* (poWW2 + poWW1 and poD3 + poD4) when calculating the preservation of the C_4 pathway because these pairs of modules had C_4-like expression patterns and were strongly connected (Figure 3, A and E). In the *P. amilis* C_4 PGNs, 86 genes (38%) were preserved (Supplemental Figure S4), which represented all core C_4 (*ALAAT*, *ASP*, *BCA*, *ME*, *MDH*, and *PPC-1E1a′*) and PEP regeneration gene families (adenylate kinase [*ADK*], sodium/pyruvate cotransporter 2 [*BASS2*], sodium–hydrogen antiporter [*NDH*], soluble inorganic pyrophosphatase [*PPA*], pyruvate, phosphate dikinase [*PPDK*], and PEP/phosphate translocator [*PPT*]). It also contained many transitory starch pathway genes that build and transport sugars and carbohydrates (e.g. *ENO*, *GAP*, phosphoglycerate kinase [*PGK*], *PGM*, and triose phosphate/phosphate translocator [*TPT*]). In addition to *PaBASS2-1* (FUN_026309), which imports pyruvate into the chloroplast as a substrate for PEP generation, we recovered two paralogs of mouse-ear cress (*Arabidopsis thaliana*) RETICULATA-RELATED (*RER*) 4 (AT5G12470). *RER* homologs have been implicated as mesophyll pyruvate importers and bundle-sheath pyruvate exporters in maize (*Zea mays*; Bräutigam et al., 2008; Friso et al., 2010; Chang et al., 2012), and thus may serve a similar function to *BASS2*. Also among the preserved genes were key enzymatic regulators (e.g. serine/threonine-protein phosphatase [*PP2A*] subunits and

RuBisCO activase [*RCA*]) and transcription factors and clock elements (e.g. CIRCADIAN CLOCK ASSOCIATED 1 [*CCA1*]).

Portulaca amilis and *P. oleracea* span a deep node in the *Portulaca* phylogeny (Figure 1C) and it was unclear which facets of C_4 they might share. A similar fraction of C_4 module genes were preserved between well-watered and drought C_4 PGNs in *P. oleracea* (117; 41.2%), and these largely consisted of the same gene families (58.3% overlap with preserved *P. amilis* C_4 gene families). We identified orthologous components of C_4 gene networks by taking the intersection of the *P. amilis* and *P. oleracea* well-watered C_4 PGNs, which contained 186 and 165 homologs, respectively, that represented 258 unique ortholog groups. Roughly, one-quarter (69/258; 26.7%) of these ortholog groups were recovered in the common C_4 networks, while 117 (45.3%) and 72 (27.9%) were exclusive to *P. amilis* and *P. oleracea*, respectively. The common networks included many of the most highly expressed copies of key C_4 genes, including the PEP generation pathway, and most of the photorespiratory pathway (Supplemental Figure S5).

Each species' C_4 PGN also contained exclusive orthologs of most C_4 gene families, some of which represent species-specific duplication events. Both species exhibited exclusive use of orthologs of *ADK*, *ALAAT*, *ASP*, *BCA*, *MDH*, *ME*, *NDH*, *PP2A*, *PPA*, mitochondrial uncoupling protein (*PUMP*), RuBisCO small subunit (*RBCS*), and *RCA*, among others. Some exclusive homologs fit biochemical expectations. Exclusive to *P. amilis* (NADP-type C_4) were three chloroplastic *NADP-ME4* paralogs (FUN_006401, FUN_006404, and FUN_006411) which did not have orthologs in the *P. oleracea* transcriptome. These three copies were on the same strand and physically close in the genome (within ~85 kb); they possibly represent tandem duplication events of *PaNADP-ME4-4* (FUN_006423), which is ~50-kb downstream of FUN_006411 (Figure 2A). These tandem duplicates had nearly identical expression profiles and were orders of magnitude more highly expressed than all other *MEs*. Tandem duplicates can have disproportionate effects because they are often expressed synchronously at magnitudes greater than expected based on their copy number (Loehlin and Carroll, 2016). It is plausible that such duplication events affected the dominance of NADP-, rather than NAD-type, enzymes in *P. amilis*. In *P. oleracea*, two *ASP* (TRINITY_DN71325_c0_g1 and TRINITY_DN346_c1_g3) and three *ALAAT* (TRINITY_DN43865_c0_g1, TRINITY_DN43865_c0_g2, and TRINITY_DN81553_c0_g1) homologs were found in orthogroups that had no *P. amilis* members. Many of the genes that were exclusive to either C_4 PGN were circadian clock and light response transcription factors, or regulatory enzymes, such as homologs of FAR-RED IMPAIRED RESPONSE, APRR, and LATE ELONGATED HYPOCOTYL (*LHY*).

We used the drought C_4 PGNs to identify orthologous ancestral elements of the daytime portion of the CAM cycle. We expected this portion of CAM to be nearly indistinguishable from C_4 (Figure 1, A and B), but to only exhibit C_4-like expression under drought stress. To be considered part of

the ancestral CAM cycle, elements needed to both be shared between the two drought C$_4$ PGNs and be significantly upregulated under drought ($q < 0.05$). Eleven orthologs met these potentially CAM-induced criteria, but only one had a function directly related to daytime malate decarboxylation: chloroplastic *NADP-ME4-5* (FUN_015913; TRINITY_DN81025_c0_g1; Figure 4O). Although only significantly drought-upregulated in *P. amilis* ($q < 0.05$; Figure 4L), the candidate vacuolar malate exporter *tonoplast dicarboxylate transporter* (*TDT*) had peak early morning abundance in both species (FUN_012199; TRINITY_DN161_c0_g1). *PUMP5-1*—also known as *dicarboxylate transporter 1*—of both species also appeared CAM induced (Figure 4M) but was not significantly differentially abundant when considering the entire time series in *P. oleracea* ($q = 0.24$). Furthermore, the *P. amilis* C$_4$ PGNs contained a drought exclusive mitochondrial *NAD-ME2-1* (FUN_037145) that was significantly upregulated ($q < 0.01$; Figure 4N), and a second, preserved ortholog (*NAD-ME1-1*; FUN_021996) that was significantly upregulated under drought ($q < 0.05$). Taken together, our findings suggest that TDT is a CAM malate exporter and that mitochondrial NAD decarboxylation may still be elicited by CAM in *P. amilis* despite NADP-type C$_4$. In contrast, constitutive expression of *PoNAD-ME1-1* and *PoNAD-ME2-1* was consistent with use in C$_4$, suggesting that *P. oleracea* may have recruited its ancestral CAM NAD-decarboxylating pathway into C$_4$. Finally, and unexpectedly, one *P. amilis* paralog of the RuBisCO small subunit B (*PaRBCS-B-1*; FUN_016561) fit a CAM induced abundance pattern ($q < 0.001$) and was expressed on the same order of magnitude as other *RBCS* homologs.

Motif identification and enrichment

Enriched motifs were detected in at least one region (i.e. 3′-untranslated region [UTR], 5′-UTR, introns, or upstream promoter) of gene models in many *P. amilis* modules. However, no enriched motifs were identified for paWW1 or paWW3—which contained the bulk of C$_4$ genes when well-watered—nor within the upstream regions of genes preserved with *PaPPC-1E1a′*. In contrast, the 5′-UTRs and upstream promoter regions of the preserved *PaPPC-1E1c* module were enriched in eight similar but nonredundant motifs ($p < 0.01$, E-value < 0.05), all of which had circadian or light response functions (Table 1). We identified a total of 80 motif matches in the 5′-UTRs of the genes comprising the *PaPPC-1E1c* module, which were distributed among 13 genes (median 7 motifs) and 24 unique, nonoverlapping regions. All motifs were annotated to Myb-related families that contained either an evening element (EE; AAAATATCT) or GATA (HGATAR) motif. EE and GATA motifs often serve as binding sites for core circadian oscillator transcription factors such as RVEs, CCA1, LHY, and APRR1, also known as TIMING OF CAB 1 (TOC1) (Reyes et al., 2004; Gendron et al., 2012; McClung, 2019). These motifs were present in 38.1%–47.6% of the sequences, and 7 of 8 enriched motifs were found in the 5′-UTR of *PaPPC-1E1c*. Some motifs were often—but not strictly—nested within others, or present on the noncoding strand. Thus, many of these regions may provide fuzzy matches or greater combinatoric control to transcription factors or other regulatory proteins.

Discussion

Plant photosynthetic adaptations can serve as models for exploring central themes of biology, such as the evolution of modularity and evolvability, gene and genome duplication, convergent evolution, and the evolution of novel phenotypes. Network analyses provide powerful tools for identifying and comparing modules of genes related to functions of interest against a background of tens of thousands of genes with complicated temporal expression patterns. C$_4$ + CAM photosynthesis has only been reported in four plant lineages, *Portulaca* (Koch and Kennedy, 1980), *Ottelia* (Hydrocharitaceae) (Zhang et al., 2013; Huang et al., 2018), *Spinifex* (Poaceae) (Ho et al., 2019), and *Trianthema* (Aizoaceae) (Winter et al., 2020), but CCMs have evolved many dozens of times (Keeley and Rundel, 2003; Edwards et al., 2010; Christin et al., 2011; Sage, 2016; Edwards, 2019) and tests for facultative CAM in C$_4$ species have only rarely been pursued. CCM evolution is a classic example of the repeated assembly of a new function via the integration of

Table 1 Motifs enriched in the 5′-UTR of genes preserved in the *PaPPC-1E1c* module

Motif name(s)	JASPAR matrix ID(s)	Consensus sequence[a]	Associated TF(s)	*Arabidopsis* ortholog(s)	E-value	Occurrences
RVE7L	MA1191.1	HHHVA**AAAATATCT**WA	RVE 7-like (RVE7L)	AT3G10113	6.09e-8	9
RVE1	MA1184.1	HHVW**AAAATATCT**WH	RVE1	AT5G17300	6.09e-5	9
RVE8	MA1182.1	**AGATAT**TTTWDD	LHY-CCA1-like 5 (LCL5)/RVE8	AT3G09600	9.21e-5	10
RVE4	MA1187.1	**AGATAT**TTTT	LHY-CCA-like 1 (LCL1)/RVE4	AT5G02840	6.96e-4	8
RVE5, RVE6	MA1190.1, MA1183.1	**AGATAT**TTTTD	RVE6, RVE5	AT5G52660, AT4G01280	8.70e-4	8
LHY1	MA1185.1	**AGATAT**TTTN	LHY1	AT1G01060	9.44e-4	10
EPR1	MA1401.1	RA**AAAATATCT**WA	Early-phytochrome-responsive 1 (EPR1)/(RVE7	AT1G18330	2.96e-3	8
CCA1	MA0972.1	**AAAATATCT**	CCA1	AT2G46830	2.28e-2	10

[a]Bold text indicates EE (AAAATATCT) or GATA (HGATAR) motifs.

multiple, existing gene networks (Heyduk et al., 2019). When coupled with patterns of transcript abundance and placed in an evolutionary context, our network results provide an initial interpretation of how these metabolic pathways interact in *Portulaca*, and how they were evolutionarily assembled.

The evolution of C_4 + CAM in *Portulaca*

Facultative CAM is ancestral to *Portulaca*, and likely evolved by coupling elements of the TCA cycle (i.e., PEPC and BCA) to the phosphorolytic starch degradation pathway via the circadian clock and increasing nocturnal PPCK activity. Our results are consistent with gene co-expression networks in *Sedum album* (Wai et al., 2019) and *Kalanchoë fedtschenkoi* (Yang et al., 2017), in which core CAM, circadian, and starch synthesis genes were tightly linked, as well as models of facultative CAM that predict transitions to phosphorolytic starch pathways during CAM induction (Shameer et al., 2018). CAM in both species was restricted to a minimal set of tightly regulated nocturnal pathways that linked *PPC-1E1c* to the transitory starch pathway, with only parts of the decarboxylation pathways distinguishable from C_4. Thus, the initial steps in CAM evolution likely involved bringing organic acid production under derived circadian control and altering *PPCK* expression in response to abiotic stress.

Shared use of some enzymes and pathways suggests that the most recent common ancestor of *Portulaca* may have had some C_4 characters. Shared photorespiratory modules, found here, and proto-C_4 anatomy in C_3–C_4 intermediate taxa (Voznesenskaya et al., 2010, 2017) suggest that C_2 metabolism—the enhanced refixation of photorespired CO_2 by preferential expression of various photorespiratory enzymes (Sage et al., 2012; Mallmann et al., 2014)—may also be ancestral to *Portulaca*. C_2 requires the partitioning of existing gene networks between bundle sheath and mesophyll cells and, in *Flaveria*, different paralogs have been co-opted or pseudogenized as distinct lineages transitioned from C_3 to C_2 to C_4 (Schulze et al., 2013). Our comparison of well-watered C_4 gene networks revealed many shared photorespiratory orthologs that may point to a single origin. However, it is difficult to distinguish between a scenario in which these orthologs were co-opted into C_2 metabolism once near the stem of extant *Portulaca*, or more recently along multiple branches in parallel. Shared use of PEPC-1E1a′ in C_4 has been hypothesized to have occurred through parallel recruitment (Christin et al., 2014), stemming from "preconditioning," such as increased expression (Moreno-Villena et al., 2018) or adaptive amino acid substitutions. C_2 metabolism is hypothesized to typically be followed by rapid evolution of C_4 (Sage et al., 2012; Mallmann et al., 2014), and, therefore, represents a limit of what we expect to be shared among *Portulaca* lineages with distinct morphologies and biochemistries. Broader sampling across the *Portulaca* phylogeny is needed to precisely delimit the shared first steps toward C_4 and subsequent parallel refinement of C_4 + CAM.

Integration of C_4 and CAM in *Portulaca*

Portulaca amilis and *P. oleracea* have canonical C_4 pathways, but constitutively operate very weak CAM cycles (at least at the transcriptional level) that are upregulated under drought. The core elements of C_4 and CAM were moderately preserved in both species, and where parts of the C_4 and CAM pathways could theoretically overlap, we often found alternative homologs. Transcript abundances do not always reflect protein abundances and activities (Baerenfaller et al., 2012; Uhrig et al., 2021); however, proteins that cycle in abundance or phosphorylation status tend to be involved in photosynthesis, light response, and carbohydrate metabolism (Uhrig et al., 2021), and research in *Agave* has found moderate to strong correlations between CAM transcripts, proteins, and metabolites (Abraham et al., 2016). Thus, taking transcript abundances of C_4 and CAM related genes as proxies for enzymatic and metabolic activity, conflicting intracellular physiological cues from CAM likely play minor roles in altering C_4 activity. Given the strong diffusion gradients between mesophyll and bundle sheath of C_4 species (Leegood, 1985), we suspect that the evolution of C_4 in *Portulaca* has resulted in two-cell CAM, as has been previously hypothesized (Lara et al., 2004), where malate produced by CAM in the mesophyll is largely decarboxylated in the bundle sheath, but it is unclear if overnight storage occurs in the mesophyll, bundle sheath, or both (Figure 6). Drought-induced upregulation of decarboxylating enzymes was consistent with expectations given C_4 biochemistries. Upregulation of mitochondrial *PaNAD-ME1-1* and *PaNAD-ME2-1* during CAM induction in *P. amilis* indicated that C_4 did not co-opt the entirety of the diurnal portion of the CAM cycle (Figure 6). In contrast, constitutive use of *PoNAD-ME1-1* and *PoNAD-ME2-1* in *P. oleracea* was consistent with recruitment and integration of the ancestral CAM NAD-decarboxylating pathway into C_4, while the NADP pathway maintained its role in CAM (Supplemental Figure S6).

Our network results confirmed that the nocturnal portion of CAM is a fixed gene network—rather than the result of drought-induced "rewiring"—that is both transcriptionally and posttranscriptionally regulated under drought to increase CAM activity. Gas exchange measurements in *Portulaca* show substantial net CO_2 loss during the night when well-watered (Holtum et al., 2017; Winter et al., 2019; Ferrari et al., 2020b, 2020c). Therefore, well-watered expression or activity of the preserved CAM-related genes are either not high enough to re-fix all nocturnally respired CO_2 or must have their products regulated at a posttranscriptional level. Evidence for the latter is given by expression patterns of *PPCK*, which was upregulated in both species under drought, and during the dark period in particular, which implies a role in increasing nocturnal PEPC activity for CAM under drought. Carter et al. (1996) hypothesized that *de novo* synthesis of PPCK may cause the PEPC diel activity in obligate CAM *Kalanchoë*. To our knowledge, similar *PPCK* transcription interference studies have not been done in a facultative CAM species and would fill a substantial knowledge gap about CAM induction. In *P. oleracea*, the
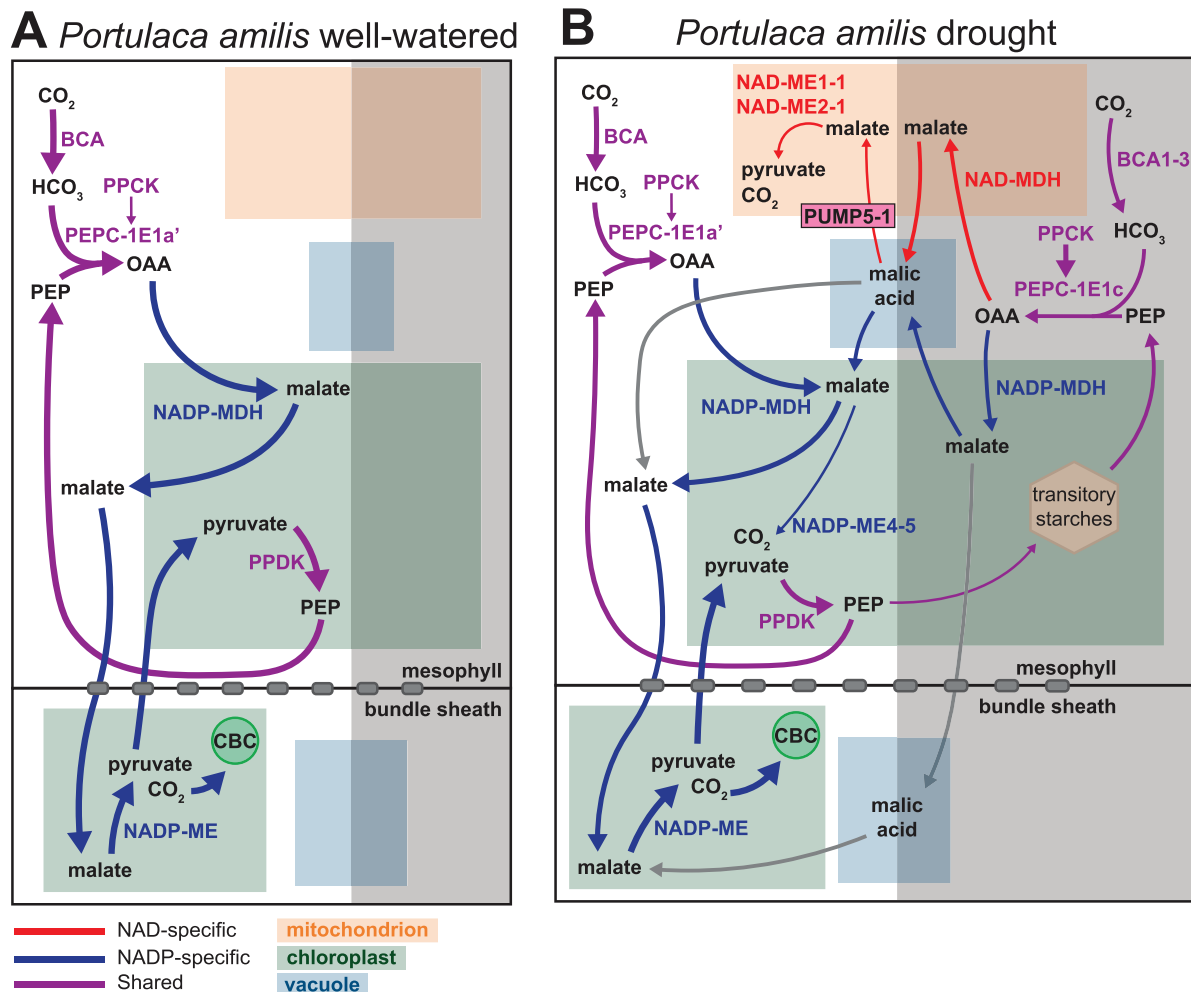
Figure 6 Hypothesized photosynthetic carbon fluxes of C_4 + CAM in *P. amilis*. Major carbon fluxes when well-watered (A) and droughted (B). Red, blue, and purple lines indicate NAD-specific, NADP specific, and shared reactions, respectively, and gray lines show possible pathways for malate that are unique to C_4 + CAM photosynthesis. Line thicknesses are indicative of relative fluxes through pathways. ALAAT, alanine aminotransferase; ASP, aspartate aminotransferase; BCA, beta carbonic anhydrase; CBC, Calvin-Benson cycle; NAD-MDH, NAD-dependent malate dehydrogenase; NAD-ME, NAD-dependent malic enzyme; NADP-MDH, NADP-dependent malate dehydrogenase; NADP-ME, NADP-dependent malic enzyme; OAA, oxaloacetate; PEP, phosphoenolpyruvate; PEPC, PEP carboxylase; PPCK, PEPC kinase; PPDK, pyruvate, phosphate dikinase.

maintenance of high daytime *PoPPCK* expression with a nocturnal peak in abundance suggests that PPCK may play a dual role in both C_4 and CAM. In contrast, we were surprised to find that *PaPPCK* had expression only consistent with use in CAM, as we are not aware of other C_4 species without high morning expression of *PPCK*; but a derived amino acid residue in PEPC-1E1a′ has the potential to increase its activity by reducing malate inhibition, as has been shown in *Kalanchoë* and *Phalaenopsis* (Yang et al., 2017). Therefore, the avoidance of pleiotropic effects has occurred through redundant homologs (e.g., decarboxylating enzymes) and adaptive mutations, but *P. oleracea* provides evidence that pleiotropy may not constrain some genes.

Portulaca as a model for metabolic evolution

Portulaca is a compelling model system for studying many evolutionary and ecophysiological questions, and its rare metabolism and experimental practicality make it a powerful

tool for genetic engineering. Forward engineering of both C_4 (Schuler et al., 2016) and CAM (Borland et al., 2014) have become priorities for agriculture as arid lands expand and populations grow. Despite the small genome size of *P. amilis*, duplication events deeper in the history of the Portulacineae (Wang et al., 2019) have played large roles in the evolution of C_4 + CAM, with implications for neofunctionalization and the evolution of modularity. With the generation of the first *Portulaca* genome, we provide a resource for studying these past events and for the functional genetic work to understand and engineer CCMs.

CAM is found in every major clade of the Portulacineae (Ting and Hanscom, 1977; Guralnick and Jackson, 2001; Guralnick et al., 2007; Edwards and Ogburn, 2012; Holtum et al., 2018; Hancock et al., 2019) (Figure 1C), and stronger and constitutive CAM have evolved in *Portulaca*'s closest relatives, Anacampserotaceae and Cactaceae (Nobel, 2003; Edwards and Donoghue, 2006; Guralnick et al., 2007). These

three clades overlap in climate space (Edwards and Ogburn, 2012) and geographical range (Eggli, 2004), show succulent morphologies capable of photosynthesis in their stems (Guralnick et al., 2007; Ogburn and Edwards, 2009), and likely share the same ancestral CAM cycle. It is still an open question why only *Portulaca* evolved C$_4$ + CAM, while stronger CAM evolved in close relatives. C$_4$ and CAM consume more energy than C$_3$ photosynthesis, and we lack models to predict environmental conditions that would select for C$_4$ in a CAM plant (or vice versa). Selection pressures to evolve C$_2$ in the facultative CAM ancestor of *Portulaca* may have been no different than in C$_3$ plants, as CAM does not necessarily reduce photorespiration, and in some cases can exacerbate it (Niewiadomska and Borland, 2008). Future progress on these topics will be made through continued study of the C$_3$–C$_4$ Cryptopetala clade that uses C$_2$ metabolism.

Despite an increased general interest in CCMs over recent years, and *Portulaca*'s C$_4$ + CAM system in particular, we have only a limited understanding of the benefits of combining C$_4$ and CAM. The advantages of facultative CAM vary between lineages, as does carbon gain, which is typically < 10% of the daytime photosynthetic activity (Herrera, 2008; Winter, 2019). However, the benefits of facultative CAM in a C$_4$ plant likely outweigh those in a C$_3$ plant. Models of facultative CAM show that productivity is generally reduced relative to C$_3$ plants over commonly observed ratios of RuBisCO carboxylation to oxygenation, but that this trend reverses as carbon concentration activity increases (Shameer et al., 2018). Thus, the use of C$_4$ in *Portulaca* may reduce photorespiration sufficiently to offset the added energy required for CAM. Facultative CAM also increases water use efficiency and can prevent reduced growth and reproductive output under drought while reducing photoinhibition (radiation induced damage to photosystems) (Herrera, 2008; Winter, 2019). Measures of chlorophyll *a* in *P. oleracea* over a water limitation experiment provide evidence that facultative CAM reduces photoinhibition (Ferrari et al., 2020b). A photoprotective role of CAM is further corroborated by rapid recovery of photosynthetic rate upon rewatering (Holtum et al., 2017; Winter et al., 2019), indicating little or no damage is done to photosystems. Gas exchange measurements also show that *Portulaca* continue to grow despite several days of drought stress (Holtum et al., 2017; Winter et al., 2019). Furthermore, drought stress may increase CO$_2$ leakiness of bundle sheath in C$_4$ plants, especially when carboxylation activity decreases relative to decarboxylation (Ghannoum, 2009). Thus, facultative CAM may supply carbon and photoprotection during drought that accelerates the transition to full photosynthetic capacity upon rewatering and allows for growth and reproduction despite large water deficits.

The annotated *P. amilis* genome and metabolic modules identified here, combined with recent resources for transgenic research in *Portulaca* (Ferrari et al., 2020a) signal a consequential shift toward the development of an experimental, functional genomics-based research program in C$_4$ + CAM. On one hand, we suggest that *P. amilis* is a better candidate than *P. oleracea* for further model system development, in part because *P. oleracea* exists within the context of a larger species complex of over a dozen described species and subspecies with uncertain relationships and multiple whole genome duplication events (Ocampo and Columbus, 2012). *Portulaca amilis* has an indistinguishable life history from *P. oleracea* (i.e., 3- to 5-week life cycle, thousands of seeds produced, self-fertilization), but does not suffer from the same taxonomic challenges and variations in ploidy. On the other hand, we view the *Portulaca* clade as providing not one, but at least three, evolutionary origins of C$_4$ + CAM systems, and there is much to be learned in understanding their similarities and differences.

Conclusions

The evolution of modularity is a common theme in studies of evolutionary development and the origin of novel phenotypes. Network-based analyses can distinguish complex and highly overlapping metabolic modules and establish their orthology between species. C$_4$ + CAM represents a unique opportunity to understand how a single module that is typically recruited into two distinct functions is regulated when both new functions operate in a single organism. Remarkably, their integration appears possible in part via further modularization, with little overlap in C$_4$ and CAM gene networks. Assignment of homologs to functions and generation of a high-quality genome for *P. amilis* were necessary first steps for future functional genetic work on C$_4$ + CAM. Perhaps the most pertinent questions surround the utility of C$_4$ + CAM, which could be addressed in part by knockdown or knockout *PPC-1E1c* lines to study the fitness of a purely C$_4$ *Portulaca*. In addition to functional genetic experiments, similar CAM-induction experiments are needed throughout *Portulaca* to establish homology between metabolic pathways across the multiple origins; especially in the C$_3$–C$_4$ Cryptopetala clade, which will further clarify the ancestral elements of C$_4$ + CAM.

Materials and methods

Plant materials and CAM-induction experiment

Specimens of *P. amilis* and *P. oleracea* were collected in Casselberry, Florida, USA and propagated in the Plant Environmental Center at Brown University. S2 seeds were germinated at Yale's Marsh Botanical Garden. One S2 *P. amilis* was removed from soil, gently washed to remove soil, flash frozen whole in liquid N$_2$, and shipped overnight to Dovetail Genomics (Scotts Valley, CA, USA) for whole-genome sequencing and assembly (see Supplemental Materials and Methods). An S4 individual was collected and vouchered at the Yale University Herbarium in the Peabody Museum of Natural History.

S3 *P. amilis* and S2 *P. oleracea* were germinated in a growth chamber with the following environmental conditions: 00:00–06:00, dark, 22°C; 06:00–20:00, lights on, 25°C;

20:00–23:59, dark, 22°C. Plants were regularly bottom watered and the mean photosynthetic photon flux density at plant level was ∼385 mol · m^{-2} · s^{-1} during the 14-h photoperiod. After ∼4 weeks, eight plants of each species were selected for CAM induction: six biological replicates and two indicator plants. Indicator plants were monitored daily for fluctuations in titratable acidity to determine CAM induction and were not included in any further analyses. To induce CAM, water was withheld from plants, and significant (one sample *t* test, $p < 0.01$) increases in nocturnal titratable acidity were observed in *P. amilis* and *P. oleracea* indicator plants after 7 and 8 days, respectively. Leaf tissue was collected from all six biological replicates for titratable acidity assays at 16:00 and 04:00 (the following day) and bulk RNA at 10:00, 16:00, 22:00, and 04:00 (the following day) on Day 0 (referred to as "well-watered") and Days 8 and 9 (referred to "drought").

Titratable acidity was assessed by boiling 0.2–0.3 g fresh leaf tissue in 60-mL 20% volume per volume EtOH until the volume was reduced by half (∼30 mL). Distilled water was then added to return the volume to 60 mL. This process was repeated, and the supernatant was then covered and allowed to cool to room temperature. Samples were then titrated to a pH of 7.0 using 0.002 M NaOH and recorded in units of μEq H$^+$ per gram fresh mass—calculated as volume titrant (μL) × titrant molarity (M)/tissue mass (g).

Total leaf RNA was extracted using Option 2 (CTAB/TRIzol/sarkosyl) from Jordon-Thaden et al. (2015). Sample purity was measured using a NanoDrop (Invitrogen by Thermo Fisher Scientific, Carlsbad, CA, USA), and a representative set of 12 samples were further assayed using a 2100 Bioanalyzer (Agilent Technologies, Santa Clara, CA, USA) for fragment length distribution and RNA integrity (RIN); RIN scores ⩾ 7 were considered high quality. Library preparation included poly (A) tailing to pull down mRNA, and sequencing was done on an Illumina HiSeq (2 × 100-bp paired-end reads), with an expected 25 million reads per sample. Four of the 96 total libraries failed during sequencing; all were *P. oleracea* samples (one 10:00 drought, one 16:00 drought, and two 04:00 drought).

Genome and transcriptome assembly and annotation

The *P. amilis* version 1 genome was assembled *de novo* by Dovetail Genomics and annotated using funannotate version 1.6.0 (http://doi.org/10.5281/zenodo.3354704) (see Supplemental Materials and Methods). Funannotate is a modular software package for genomic scaffold cleaning, genomic element prediction (i.e. genes, UTRs, tRNAs, etc.), functional annotation, and comparative genomics; a step-by-step walkthrough of the entire annotation process can be found on GitHub (https://github.com/isgilman/Portulaca-amilis-genome).

The *de novo P. oleracea* transcriptome was assembled using Trinity version 2.11.0 (Grabherr et al., 2011). We reduced the redundancy of the resulting contigs using CD-HIT version 4.8.1 (Fu et al., 2012) by collapsing contigs with at least 98% similarity (-c 98) and open reading frames were identified with TransDecoder. Orthology between *P. amilis* and *P. oleracea* peptide sequences was established using OrthoFinder (Emms and Kelly, 2015) version 2.5.2 and the primary peptide sequences from genomes of pineapple (*A. comosus*), *Amaranthus hypochondriacus*, mouse-ear cress (*A. thaliana*), *Brachypodium distachyon*, common sunflower (*Helianthus annuus*), *Kalanchoë fedtschenkoi*, *Phalaenopsis equestris*, white stonecrop (*S. album*), sorghum (*Sorghum bicolor*), common grape (*Vitis vinifera*), and maize (*Zea mays*) (Supplemental Data Sets 1 and 2).

RNAseq differential abundance analysis

We used sleuth (Pimentel et al., 2017) version 0.30.0 in R version 3.6.1 to assess differential abundance of RNAseq reads quantified by Kallisto for each species independently. For *P. amilis*, we mapped reads to the predicted mRNA transcripts from the genome annotation, and for *P. oleracea* we used the redundancy reduced *de novo* transcriptome. All analyses were conducted at the gene level by providing a transcript-to-gene map to sleuth generated from the final set of gene models and setting "gene_mode" = TRUE. Abundance data were quantified in transcripts per million (TPM) and differential abundance was assessed using a likelihood ratio test between the reduced design matrix, where abundance was purely a function of sampling time ("y ∼ time_point"), and the full design matrix that included time and water treatment ("y ∼ time_point + treatment"). *P*-values for unique transcripts were aggregated for each gene model and transformed into *q*-values by adjusting for false discovery rate (Benjamini–Hochberg correction).

Co-expression network analysis

We used Weighted Gene Correlation Network Analysis (WGCNA) (Langfelder and Horvath, 2008) version 1.69 in R version 3.6.1 to construct co-expression networks and identify modules, and NetworkX (Hagberg et al., 2008) version 2.5 in Python version 3.7.3 to visualize and measure network features. WGCNA was run separately for each species and condition using TPM-normalized abundance data for all biological replicates, resulting in four networks, and genes were categorized according to their primary roles in photosynthesis (see Supplemental Materials and Methods).

Motif identification and enrichment

Putative *cis*-regulatory motif identification and enrichment was done using the MEME Suite (Bailey et al., 2009) version 5.0.2. First, 5′- and 3′-UTRs, introns, and 2-kb upstream regions were extracted from all *P. amilis* gene models. The MEME tool (Bailey and Elkan, 1994) was used to identify *de novo* motifs for each co-expression module and region using an *E*-value threshold of 0.05 and a minimum motif size of 6 bp. We downloaded the JASPAR CORE 2018 motif database (Khan et al., 2018), supplemented it with the *de novo* motifs identified in (Wai et al. (2019) related to CAM, and finally added *de novo P. amilis* motifs after checking for

redundancy with Tomtom (Gupta et al., 2007). We then used AME (–scoring avg –method fisher –hit-lo-fraction 0.25 –evalue-report-threshold 0.05) (McLeay and Bailey, 2010) with random sets of control sequences to measure motif enrichment in every module–region combination, as well as the preserved genes of the *PPC-1E1c* and C₄ modules. Precise locations of motif occurrences were determined using FIMO (Grant et al., 2011).

Data availability

Genomic scaffolds, peptide and coding sequences, assembled transcriptome, and annotations (including repeats) for *P. amilis* are available through the Phytozome web portal (https://phytozome-next.jgi.doe.gov/info/Pamilis_v1_0). Raw RNAseq data for *P. amilis* and *P. oleracea* are available through the NCBI's SRA within BioProject PRJNA732408.

Code availability

Walkthroughs of genome annotation and RNAseq analyses (including differential abundance and co-expression network analyses) and all custom code are available on GitHub at https://github.com/isgilman/Portulaca-amilis-genome and https://github.com/isgilman/Portulaca-coexpression, respectively.

Accession numbers

Sequence data from this article can be found in the GenBank/EMBL data libraries under accession number PRJNA732408. Additional information for all genes/proteins mentioned in this text, including annotations, module assignments, and orthology to *A. thaliana* can be found in Supplemental Data Sets 1 and 2.

Supplemental data

The following materials are available in the online version of this article.

Supplemental Figure S1. Gene co-expression network module size distributions.

Supplemental Figure S2. *Portulaca amilis* transcript abundance for all gene families discussed in the text.

Supplemental Figure S3. *Portulaca oleracea* transcript abundance for all gene families discussed in the text.

Supplemental Figure S4. Preservation of C₄ PGNs.

Supplemental Figure S5. Common well-watered C₄ PGNs.

Supplemental Figure S6. Hypothesized photosynthetic carbon fluxes of C₄ + CAM in *P. oleracea*.

Supplemental Table S1. PGN summary statistics.

Supplemental Methods S1. Genome and transcriptome assembly and annotation.

Supplemental Methods S2. Co-expression network analysis.

Supplemental Data Set 1. *Portulaca amilis* photosynthesis related gene annotations with functional categorizations and module assignments.

Supplemental Data Set 2. *Portulaca oleracea* photosynthesis related gene annotations with functional categorizations and module assignments.

Supplemental Data Set 3. Orthogroup assignments.

Supplemental Data Set 4. Orthogroup gene trees.

References

Abraham PE, Yin H, Borland AM, Weighill D, Lim SD, Paoli HCD, Engle N, Jones PC, Agh R, Weston DJ, et al. (2016) Transcript, protein and metabolite temporal dynamics in the CAM plant Agave. Nat Plants **2**: 16178

Arakaki M, Christin PA, Nyffeler R, Lendel A, Eggli U, Ogburn RM, Spriggs E, Moore MJ, Edwards EJ (2011) Contemporaneous and recent radiations of the world's major succulent plant lineages. Proc Nat Acad Sci USA **108**: 8379–8384

Baerenfaller K, Massonnet C, Walsh S, Baginsky S, Bühlmann P, Hennig L, Hirsch-Hoffmann M, Howell KA, Kahlau S, Radziejwoski A, et al. (2012) Systems-based analysis of Arabidopsis leaf growth reveals adaptation to water deficit. Mol Syst Biol **8**: 606–606

Bailey TL, Boden M, Buske FA, Frith M, Grant CE, Clementi L, Ren J, Li WW, Noble WS (2009) MEME Suite: tools for motif discovery and searching. Nucleic Acids Res **37**: W202–W208

Bailey TL, Elkan C (1994) Fitting a mixture model by expectation maximization to discover motifs in biopolymers. Proceedings of the Second International Conference on Intelligent Systems for Molecular Biology. AAAI Press, Menlo Park, CA, pp 28–36

Barve A, Wagner A (2013) A latent capacity for evolutionary innovation through exaptation in metabolic systems. Nature **500**: 203–206

Benjamini Y, Hochberg Y (1995) Controlling the false discovery date: a practical and powerful approach to multiple testing. J Royal Stat Soc Ser B Methodol **57**: 289–300

Borland AM, Guo HB, Yang X, Cushman JC (2016) Orchestration of carbohydrate processing for crassulacean acid metabolism. Curr Opin Plant Biol **31**: 118–124

Borland AM, Hartwell J, Weston DJ, Schlauch KA, Tschaplinski TJ, Tuskan GA, Yang X, Cushman JC (2014) Engineering crassulacean acid metabolism to improve water-use efficiency. Trends Plant Sci **19**: 327–338

Bräutigam A, Hoffmann-Benning S, Weber APM (2008) Comparative proteomics of chloroplast envelopes from C₃ and C₄ plants reveals specific adaptations of the plastid envelope to C₄ photosynthesis and candidate proteins required for maintaining C₄ metabolite fluxes. Plant Physiol **148**: 568–579

Bräutigam A, Schlüter U, Eisenhut M, Gowik U (2017) On the evolutionary origin of CAM photosynthesis. Plant Physiol **174**: 473–477

Brilhaus D, Bräutigam A, Mettler-Altmann T, Winter K, Weber APM (2016) Reversible burst of transcriptional changes during induction of crassulacean acid metabolism in *Talinum triangulare*. Plant Physiol 170: 102–122

Carter PJ, Fewson CA, Nimmo GA, Nimmo HG, Wilkins MB (1996) Roles of circadian rhythms, light and temperature in the regulation of phosphoenolpyruvate carboxylase in crassulacean acid metabolism. *In* K Winter, JA Smith, eds, Crassulacean Acid Metabolism. Biochemistry, Ecophysiology and Evolution. Vol. 114. Springer, Berlin, Germany, pp 46–52

Ceusters N, Ceusters J, Hurtado-Castano N, Dever LV, Boxall SF, Kneřová J, Waller JL, Rodick R, Ende WV den, Hartwell J, et al. (2021) Phosphorolytic degradation of leaf starch via plastidic α-glucan phosphorylase leads to optimized plant growth and water use efficiency over the diel phases of Crassulacean acid metabolism. J Exp Bot 72: 4419–4434

Chang YM, Liu WY, Shih ACC, Shen MN, Lu CH, Lu MYJ, Yang HW, Wang TY, Chen SCC, Chen SM, et al. (2012) Characterizing regulatory and functional differentiation between maize mesophyll and bundle sheath cells by transcriptomic analysis. Plant Physiol 160: 165–177

Christin PA, Arakaki M, Osborne CP, Bräutigam A, Sage RF, Hibberd JM, Kelly S, Covshoff S, Wong GKS, Hancock L, et al. (2014) Shared origins of a key enzyme during the evolution of C$_4$ and CAM metabolism. J Exp Bot 65: 3609–3621

Christin PA, Osborne CP, Sage RF, Arakaki M, Edwards EJ (2011) C$_4$ eudicots are not younger than C$_4$ monocots. J Exp Bot 62: 3171–3181

Clune J, Mouret JB, Lipson H (2013) The evolutionary origins of modularity. Proc R Soc B Biol Sci 280: 20122863

Dion-Côté A-M, Renaut S, Normandeau E, Bernatchez L (2014) RNA-seq reveals transcriptomic shock involving transposable elements reactivation in hybrids of young lake whitefish species. Mol Biol Evol 31: 1188–1199

Edwards EJ (2019) Evolutionary trajectories, accessibility and other metaphors: the case of C$_4$ and CAM photosynthesis. New Phytologist 223: 1742–1755

Edwards EJ, Diaz M (2006) Ecological physiology of *Pereskia guamacho*, a cactus with leaves. Plant Cell Environ 29: 247–256

Edwards EJ, Donoghue MJ (2006) *Pereskia* and the origin of the cactus life-form. Am Nat 167: 777–793

Edwards EJ, Ogburn RM (2012) Angiosperm responses to a low-CO$_2$ world: CAM and C$_4$ photosynthesis as parallel evolutionary trajectories. Int J Plant Sci 173: 724–733

Edwards EJ, Osborne CP, Strömberg CAE, Smith SA, Consortium CG, Bond WJ, Christin P-A, Cousins AB, Duvall MR, Fox DL, et al. (2010) The origins of C$_4$ grasslands: integrating evolutionary and ecosystem science. Science 328: 587–591

Eggli U (2004) Illustrated Handbook of Succulent Plants: Dicotyledons. Springer, Berlin, Heidelberg, Germany

Ehleringer JR, Cerling TE, Helliker BR (1997) C$_4$ photosynthesis, atmospheric CO$_2$, and climate. Oecologia 112: 285–299

Emms DM, Kelly S (2015) OrthoFinder: solving fundamental biases in whole genome comparisons dramatically improves orthogroup inference accuracy. Genome Biol 16: 157

Ferrari RC, Bittencourt PP, Nagumo PY, Oliveira WS, Rodrigues MA, Hartwell J, Freschi L (2020a) Developing *Portulaca oleracea* as a model system for functional genomics analysis of C$_4$/CAM photosynthesis. Funct Plant Biol 7: 666–682

Ferrari RC, Bittencourt PP, Rodrigues MA, Moreno-Villena JJ, Alves FRR, Gastaldi VD, Boxall SF, Dever LV, Demarco D, Andrade SCS, et al. (2020b) C$_4$ and crassulacean acid metabolism within a single leaf: deciphering key components behind a rare photosynthetic adaptation. New Phytol 225: 1699–1714

Ferrari RC, Cruz BC, Gastaldi VD, Storl T, Ferrari EC, Boxall SF, Hartwell J, Freschi L (2020c) Exploring C$_4$-CAM plasticity within the *Portulaca oleracea* complex. Sci Rep 10: 14237–14

Friso G, Majeran W, Huang M, Sun Q, van Wijk KJ (2010) Reconstruction of metabolic pathways, protein expression, and homeostasis machineries across maize bundle sheath and mesophyll chloroplasts: large-scale quantitative proteomics using the first maize genome assembly. Plant Physiol 152: 1219–1250

Fu L, Niu B, Zhu Z, Wu S, Li W (2012) CD-HIT: accelerated for clustering the next-generation sequencing data. Bioinformatics 28: 3150–3152

Furbank RT (2011) Evolution of the C$_4$ photosynthetic mechanism: are there really three C$_4$ acid decarboxylation types? J Exp Bot 62: 3103–3108

Gendron JM, Pruneda-Paz JL, Doherty CJ, Gross AM, Kang SE, Kay SA (2012) *Arabidopsis* circadian clock protein, TOC1, is a DNA-binding transcription factor. Proc Nat Acad Sci USA 109: 3167–3172

Ghannoum O (2009) C$_4$ photosynthesis and water stress. Annals of Bot 103: 635–644

Grabherr MG, Haas BJ, Yassour M, Levin JZ, Thompson DA, Amit I, Adiconis X, Fan L, Raychowdhury R, Zeng Q, et al. (2011) Full-length transcriptome assembly from RNA-Seq data without a reference genome. Nat Biotech 29: 644–652

Grant CE, Bailey TL, Noble WS (2011) FIMO: Scanning for occurrences of a given motif. Bioinformatics 27: 1017–1018

Gupta S, Stamatoyannopoulos JA, Bailey TL, Noble WS (2007) Quantifying similarity between motifs. Genome Biol 8: R24

Guralnick LJ, Cline A, Smith M, Sage RF (2007) Evolutionary physiology: the extent of C$_4$ and CAM photosynthesis in the genera *Anacampseros* and *Grahamia* of the Portulacaceae. J Exp Bot 59: 1735–1742

Guralnick LJ, Edwards G, Ku MSB, Hockema B, Franceschi VR (2002) Photosynthetic and anatomical characteristics in the C$_4$-crassulacean acid metabolism-cycling plant, *Portulaca grandiflora*. Funct Plant Biol 29: 763–773

Guralnick LJ, Jackson MD (2001) The occurrence and phylogenetics of Crassulacean acid metabolism in the Portulacaceae. Int J Plant Sci 162: 257–262

Hagberg AA, Schult DA, Swart PJ (2008) Exploring network structure, dynamics, and function using networkX. *In* G Varopuax, T Vaught, J Millman, eds, Proceedings of the 7th Python in Science Conference (SciPy 2008). Pasadena, CA, pp 11–16

Hancock LP, Holtum JAM, Edwards EJ (2019) The evolution of CAM photosynthesis in Australian *Calandrinia* reveals lability in C$_3$ + CAM phenotypes and a possible constraint to the evolution of strong CAM. Integr Comp Biol 59: 517–534

Hartwell J (2006) The circadian clock in CAM plants. *In* AJW Hall, H McWatters, eds, Annual Plant Reviews, Vol. 21: Endogenous Plant Rhythms. Blackwell Publishing Ltd, Hoboken, NJ, pp 211–236

Herrera A (2008) Crassulacean acid metabolism and fitness under water deficit stress: if not for carbon gain, what is facultative CAM good for? Annals of Bot 103: 645–653

Heyduk K, Moreno-Villena JJ, Gilman IS, Christin PA, Edwards EJ (2019) The genetics of convergent evolution: insights from plant photosynthesis. Nat Rev Gen 313: 1–9

Hibberd JM, Covshoff S (2010) The regulation of gene expression required for C$_4$ photosynthesis. Ann Rev Plant Biol 61: 181–207

Ho CL, Chiang JM, Lin TC, Martin CE (2019) First report of C$_4$/CAM-cycling photosynthetic pathway in a succulent grass, *Spinifex littoreus* (Brum. f.) Merr., in coastal regions of Taiwan. Flora 254: 194–202

Holtum JAM, Hancock LP, Edwards EJ, Winter K (2017) Optional use of CAM photosynthesis in two C$_4$ species, *Portulaca cyclophylla* and *Portulaca digyna*. J Plant Physiol 214: 91–96

Holtum JAM, Hancock LP, Edwards EJ, Winter K (2018) Crassulacean acid metabolism in the Basellaceae (Caryophyllales). Plant Biol 20: 409–414

Holtum JAM, Hancock LP, Edwards EJ, Winter K (2021) CAM photosynthesis in desert blooming *Cistanthe* of the Atacama, Chile. Funct Plant Biol 48: 691–702

Huang WM, Shao H, Zhou SN, Zhou Q, Fu WL, Zhang T, Jiang H-S, Li W, Gontero B, Maberly SC (2018) Different CO_2 acclimation strategies in juvenile and mature leaves of *Ottelia alismoides*. Photosynth Res **138**: 219–232

Jordon-Thaden IE, Chanderbali AS, Gitzendanner MA, Soltis DE (2015) Modified CTAB and TRIzol protocols improve RNA extraction from chemically complex embryophyta. App Plant Sci **3**: 1400105–1400122

Kashtan N, Alon U (2005) Spontaneous evolution of modularity and network motifs. Proc Nat Acad Sci USA **102**: 13773–13778

Kashtan N, Noor E, Alon U (2007) Varying environments can speed up evolution. Proc Nat Acad Sci USA **104**: 13711–13716

Keeley JE, Rundel PW (2003) Evolution of CAM and C_4 carbon-concentrating mechanisms. Int J Plant Sci **164**: S55–S77

Khan A, Fornes O, Stigliani A, Gheorghe M, Castro-Mondragon JA, van der Lee R, Bessy A, Chèneby J, Kulkarni SR, Tan G, et al. (2018) JASPAR 2018: update of the open-access database of transcription factor binding profiles and its web framework. Nucleic Acids Res **46**: D260–266

Koch K, Kennedy RA (1980) Characteristics of crassulacean acid metabolism in the succulent C_4 dicot, *Portulaca oleracea* L. Plant Physiol **65**: 193–197

Koch KE, Kennedy RA (1982) Crassulacean acid metabolism in the succulent C_4 dicot, *Portulaca oleracea* L under natural environmental conditions. Plant Physiol **69**: 757–761

Langfelder P, Horvath S (2008) WGCNA: an R package for weighted correlation network analysis. BMC Bioinformatics **9**: 559

Lara MV, Disante KB, Podestá FE, Andreo CS, Drincovich MF (2003) Induction of a Crassulacean acid like metabolism in the C_4 succulent plant, *Portulaca oleracea* L.: physiological and morphological changes are accompanied by specific modifications in phosphoenolpyruvate carboxylase. Photosynth Res **77**: 241

Lara MV, Drincovich MF, Andreo CS (2004) Induction of a crassulacean acid-like metabolism in the C_4 succulent plant, *Portulaca oleracea* L.: study of enzymes involved in carbon fixation and carbohydrate metabolism. Plant Cell Physiol **45**: 618–626

Leegood RC (1985) The intercellular compartmentation of metabolites in leaves of *Zea mays* L. Planta **164**: 163–171

Lenski RE, Ofria C, Pennock RT, Adami C (2003) The evolutionary origin of complex features. Nature **423**: 139–144

Loehlin DW, Carroll SB (2016) Expression of tandem gene duplicates is often greater than twofold. Proc Nat Acad Sci **113**: 5988–5992

Lüttge U (2011) Photorespiration in phase III of crassulacean acid metabolism: evolutionary and ecophysiological implications. *In* U Lüttge, W Beyschlag, B Büdel, D Francis, eds, Progress in Botany. Springer, Berlin, Heidelberg, Germany, pp 371–384

Mallmann J, Heckmann D, Bräutigam A, Lercher MJ, Weber APM, Westhoff P, Gowik U (2014) The role of photorespiration during the evolution of C_4 photosynthesis in the genus Flaveria. eLife **3**: e02478

McClintock B (1984) The significance of responses of the genome to challenge. Science **226**: 792–801

McClung C (2019) The plant circadian oscillator. Biology **8**: 14–17

McLeay RC, Bailey TL (2010) Motif enrichment analysis: a unified framework and an evaluation on ChIP data. BMC Bioinformatics **11**: 165

Moreno-Villena JJ, Dunning LT, Osborne CP, Christin P-A (2018) Highly expressed genes are preferentially co-opted for C_4 photosynthesis. Mol Biol Evol **35**: 94–106

Niewiadomska E, Borland AM (2008) Crassulacean acid metabolism: a cause or consequence of oxidative stress in planta? *In* U Lüttge, WB Beyschlag, J Murata, eds, Progress in Botany. Springer-Verlag, Berlin, Germany, pp 247–266

Nimmo HG (2000) The regulation of phosphoenolpyruvate carboxylase in CAM plants. Trends Plant Sci **5**: 75–80

Nobel PS (2003) Environmental Biology of Agaves and Cacti. Cambridge University Press, Cambridge

Ocampo G, Columbus JT (2012) Molecular phylogenetics, historical biogeography, and chromosome number evolution of *Portulaca* (Portulacaceae). Mol Phy Evol **63**: 97–112

Ocampo G, Koteyeva NK, Voznesenskaya EV, Edwards GE, Sage TL, Sage RF, Columbus JT (2013) Evolution of leaf anatomy and photosynthetic pathways in Portulacaceae. Am J Bot **100**: 2388–2402

Ogburn RM, Edwards EJ (2009) Anatomical variation in Cactaceae and relatives: trait lability and evolutionary innovation. Am J Bot **96**: 391–408

Ogren WL (1984) Photorespiration: pathways, regulation, and modification. Ann Rev Plant Physiol **35**: 415–442

Peterhansel C, Horst I, Niessen M, Blume C, Kebeish R, Kürkcüoglu S, Kreuzaler F (2010) Photorespiration. The Arabidopsis Book **8**: e0130

Pimentel H, Bray NL, Puente S, Melsted P, Pachter L (2017) Differential analysis of RNA-seq incorporating quantification uncertainty. Nat Methods **14**: 687–690

Raven JA, Spicer RA (1996) The evolution of crassulacean acid metabolism. *In* K Winter, Smith JAC, eds, Crassulacean Acid Metabolism Biochemistry, Ecophysiology and Evolution. Springer, Berlin, Germany, pp 360–388

Reyes JC, Muro-Pastor MI, Florencio FJ (2004) The GATA family of transcription factors in *Arabidopsis* and rice. Plant Physiol **134**: 1718–1732

Sage RF (2016) A portrait of the C_4 photosynthetic family on the 50th anniversary of its discovery: species number, evolutionary lineages, and Hall of Fame. J Exp Bot **67**: 4039–4056

Sage RF (2002) Are crassulacean acid metabolism and C_4 photosynthesis incompatible? Funct Plant Biol **29**: 775–785

Sage RF (2004) The evolution of C_4 photosynthesis. New Phyt **161**: 341–370

Sage RF, Sage TL, Kocacinar F (2012) Photorespiration and the evolution of C_4 photosynthesis. Ann Rev Plant Biol **63**: 19–47

Schuler ML, Mantegazza O, Weber APM (2016) Engineering C_4 photosynthesis into C_3 chassis in the synthetic biology age. Plant Cell **87**: 51–65

Schulze S, Mallmann J, Burscheidt J, Koczor M, Streubel M, Bauwe H, Gowik U, Westhoff P (2013) Evolution of C4 photosynthesis in the genus *Flaveria*: establishment of a photorespiratory CO_2 pump. Plant Cell **25**: 2522–2535

Shameer S, Baghalian K, Cheung CYM, Ratcliffe RG, Sweetlove LJ (2018) Computational analysis of the productivity potential of CAM. Nat Plants **4**: 165–171

Sharma AK, Bhattacharyya NK (1956) Cytogenetics of some members of Portulacaceae and related families. Caryologia **8**: 257–274

Smith AM, Zeeman SC, Smith SM (2005) Starch degradation. Ann Rev Plant Biol **56**: 73–98

Szarek SR, Ting IP (1975) Photosynthetic efficiency of CAM plants in relation to C_3 and C_4 plants. *In* R Marcelle, ed, Environmental and Biological Control of Photosynthesis. Dr. W. Junk b.v., The Hague, The Netherlands, pp 289–299

Taylor SH, Ripley BS, Martin T, De-Wet L, Woodward FI, Osborne CP (2014) Physiological advantages of C4 grasses in the field: a comparative experiment demonstrating the importance of drought. Global Change Biol **20**: 1992–2003

Ting IP, Hanscom Z (1977) Induction of acid metabolism in *Portulacaria afra*. Plant Physiol **59**: 511–514

Uhrig RG, Echevarría-Zomeño S, Schlapfer P, Grossmann J, Roschitzki B, Koerber N, Fiorani F, Gruissem W (2021) Diurnal dynamics of the Arabidopsis rosette proteome and phosphoproteome. Plant Cell Environ **44**: 821–841

Voznesenskaya EV, Koteyeva NK, Edwards GE, Ocampo G (2010) Revealing diversity in structural and biochemical forms of C_4 photosynthesis and a C_3-C_4 intermediate in genus *Portulaca* L. (Portulacaceae). J Exp Bot **61**: 3647–3662

Voznesenskaya EV, Koteyeva NK, Edwards GE, Ocampo G (2017) Unique photosynthetic phenotypes in *Portulaca* (Portulacaceae): C3-C4 intermediates and NAD-ME C_4 species with Pilosoid-type Kranz anatomy. J Exp Bot **68**: 225–239

Wagner GP, Altenberg L (1996) Perspective: complex adaptations and the evolution of evolvability. Evolution **50**: 967–976

Wai CM, Weise SE, Ozersky P, Mockler TC, Michael TP, VanBuren R (2019) Time of day and network reprogramming during drought induced CAM photosynthesis in *Sedum album*. PLoS Genetics **15**: e1008209

Wang N, Yang Y, Moore MJ, Brockington SF, Walker JF, Brown JW, Liang B, Feng T, Edwards C, Mikenas J, et al. (2019) Evolution of portulacineae marked by gene tree conflict and gene family expansion associated with adaptation to harsh environments. Mol Biol Evol **36**: 112–126

Weise SE, Wijk KJ van, Sharkey TD (2011) The role of transitory starch in C$_3$, CAM, and C$_4$ metabolism and opportunities for engineering leaf starch accumulation. J Exp Bot **62**: 3109–3118

Wickell D, Kuo LY, Yang HP, Ashok AD, Irisarri I, Dadras A, Vries S de, Vries J de, Huang YM, Li Z, et al. (2021) Underwater CAM photosynthesis elucidated by *Isoetes genome*. Nat Commun **12**: 6348

Williams BP, Johnston IG, Covshoff S, Hibberd JM (2013) Phenotypic landscape inference reveals multiple evolutionary paths to C$_4$ photosynthesis. eLife **2**: e00961

Winter K (2019) Ecophysiology of constitutive and facultative CAM photosynthesis. J Exp Bot **2**: 16178–14

Winter K, Aranda J, Holtum JAM (2005) Carbon isotope composition and water-use efficiency in plants with Crassulacean acid metabolism. Funct Plant Biol **32**: 381–388

Winter K, Garcia M, Virgo A, Ceballos J, Holtum JAM (2020) Does the C$_4$ plant *Trianthema portulacastrum* (Aizoaceae) exhibit weakly expressed crassulacean acid metabolism (CAM)? Funct Plant Biol **48**: 655–665

Winter K, Sage RF, Edwards EJ, Virgo A, Holtum JAM (2019) Facultative crassulacean acid metabolism in a C$_3$-C$_4$ intermediate. J Exp Bot **108**: 8379–9

Yang X, Hu R, Yin H, Jenkins J, Shu S, Tang H, Liu D, Weighill DA, Yim WC, Ha J, et al. (2017) The *Kalanchoë* genome provides insights into convergent evolution and building blocks of crassulacean acid metabolism. Nat Commun **8**: 1–15

Zhang Y, Yin L, Jiang H-S, Li W, Gontero B, Maberly SC (2013) Biochemical and biophysical CO$_2$ concentrating mechanisms in two species of freshwater macrophyte within the genus *Ottelia* (Hydrocharitaceae). Photosynth Res **121**: 285–297

Zhao T, Schranz ME (2019) Network-based microsynteny analysis identifies major differences and genomic outliers in mammalian and angiosperm genomes. Proc Nat Acad Sci USA **116**: 2165–2174